Review Article

Single Molecule Spectroscopy

Tatiana Yu. Latychevskaia[a], Kuo Kan Liang[b]* (梁國淦), Michitoshi Hayashi[b],
Chung-Hung Chang[b] (張仲宏), Alois Renn[a], Urs. P. Wild[a],
Jui-Hung Hsu[b] (徐瑞鴻), Ta-Chau Chang[b] (張大釗) and Sheng Hsien Lin[b] (林聖賢)
[a]*Physical Chemistry Laboratory, Swiss Federal Institute of Technology,*
ETH Zentrum, CH-8092 Z ich, Switzerland
[b]*Institute of Atomic and Molecular Sciences, Academia Sinica, P. O. Box 23-166, Taipei 106, Taiwan, R.O.C.*

Single molecular experiments carried out in the group of Prof. Wild in ETH Zurich, as well as the experimental and theoretical studies of several research groups in Taiwan, have been summarized in this review. It is shown that with the contemporary technologies, single molecular experiments can be carried out under a broad range of physical conditions. These includes low and room temperatures; in vacuum, in solution, in the air, or with specific pressure applied on the sample; in applied direct-current or alternating-current electric fields; on molecules in solid matrices, in gel, or even functioning biomolecules in vitro. Theoretical efforts have been able to help identifying the interactions of single molecules with their surroundings that modulate their static or time-resolved spectroscopic properties. The joint experimental and theoretical effort to develop the research techniques in single molecular experiments is shown to be fruitful, and future works in this direction are important for many fields in chemistry, physics, and biology.

Keywords: Single molecule experiment; Spectral jump; Stark effect; ATP synthase.

1. INTRODUCTION

The efforts of chemical and physical scientists to explore the behavior of individual molecules have been manifold. Molecular beam techniques were developed to investigate effectively isolated molecules or isolated product-molecule pairs in gas phase with well defined conditions of the molecules under study. The data collected in such experiments are nevertheless ensemble data in nature. Optical or magnetic trapping techniques (commonly referred to as optical or magnetic tweezers) as well as STM or AFM manipulations of atoms and molecules allow us to observe fixed single atoms or molecules in space, in more varieties of environments like on surfaces or in solids or solutions. In these experiments, mechanical forces are involved either to access a single molecule or to detect the mechanical or elasticity properties of single molecule (SM) systems. Meanwhile, many inspiring ideas showed that actually single molecules can be observed in conditions similar to that of conventional ensemble experiments in a less difficult way than imagined. Conventional spectroscopic and microscopic techniques can be employed, with some modifications and improvements, to achieve the goal. The most important idea in this type of experiments is that, to observe a single molecule, we need to make sure that in the volume in which the probing system acts on there be only one molecule we want to study. In principle, it can be achieved by reducing the sample molecule concentration and then using spectroscopic methods, that is, the molecule under study can be picked up by monitoring a specific light-matter interaction process which occurs on the sample molecule, but not on the other surrounding molecules. In such so-called *single molecule spectroscopy* (SMS) studies, generally the difficulty in achieving single-molecular observations is not the observation of single molecules themselves, but is the rejection of unwanted information from the environment. In an earlier review,[1] the practical considerations of the experimental conditions are discussed in detail.

The possibility of assigning each molecule with a different spectroscopic property by manipulating its environment also has potential applications. For example, if the mod-

This review paper is based on the plenary lecture given by Prof. U. P. Wild at the Second Worldwide Chinese Theoretical and Computational Chemistry Conference in Taipei. The choice of scientific subjects for the article has been made by T. Latychevskaia and K. K. Liang. The discussed topics reflect the interests of several research groups in Taiwan and the Swiss group of Prof. U. P. Wild.

ifications on the properties of individual molecule can be 'remembered' by these molecules and be 'read out' later, then we may use these molecules for information storage, or they can even be used as devices for "molecular computation". That is, ability to actively manipulate the single molecules extends the range of application of these techniques to more practical usages.

From the theoretical point of view, we can briefly outline the important information that SMS studies can provide in the following:

1. The spectral properties of an SM or a certain number of SMs before ensemble average is made, in which the inhomogeneities are suppressed and can be recovered by averaging over many SMs;

2. Influence on SMs by controlled external parameters such as temperature, pressure, electric field, or even the presence of reactive species such as oxidant or deoxidant in the environment;

3. Rrandom dynamics of the spectral properties of SMs induced by fluctuations of the surroundings that can only be measured accurately in SMS experimental conditions;

4. Time trajectory of the observation of some properties which can be used to deduce the kinetics of an SM from the time domain information directly.

In the following sections, we shall focus our attention on several typical SMS experiments that have been conducted or even first developed in the authors' group, based on the plenary lecture by Prof. U. P. Wild at the Second Worldwide Chinese Theoretical and Computational Chemistry Conference in Academia Sinica, Taipei. The efforts of many other colleagues in the same field are so numerous that they cannot all be included in this review. We shall cite relevant literatures to help readers to get more detailed information or as support for the ideas. Those works not mentioned in this review were left out only due to the limited scope of this article. On the other hand, even though the details of the experimental setup are a very important and interesting part of the SM studies, they cannot fit into one review article. In this paper, we often point the readers to the theses written by members from this group for more details. Most of the theses cited can be obtained from the *Dissertations Online* service provided by ETH Zurich. The URL is http://e-collection.ethbib.ethz.ch/diss/.

2. LOW TEMPERATURE STUDIES OF SINGLE MOLECULES IN SOLIDS

The spectrum of an organic compound in a solid is a broad (hundreds or thousands wavenumbers) Gaussian line, made up of a broad distribution of single-absorber lines.[2,3] The absorption resonance frequency of individual molecules are defined by the local environment of the molecules (See Fig. 1). Figure 2 shows a simulated inhomogeneous lineshape produced by the superposition of a large number of individual homogeneous absorption profiles. When the concentration of the guest molecules in a solid is high, the sample spectrum is structureless. At a lower concentration the spectrum becomes more "noisy" and this noise is nothing other than the summed-up spectra of single absorbers at each frequency position. In

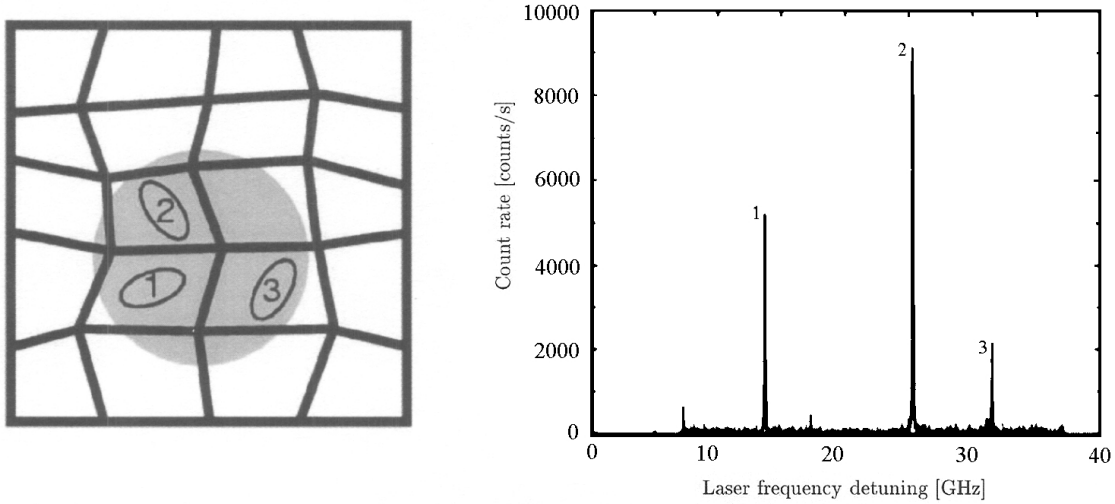

Fig. 1. Every molecule has a slightly different environment and the resonance absorption frequencies differ from molecule to molecule. The light grey circle indicates the excitation spot. The spectra in the right panel are real data.[6]

contrast to spectral noise, these spectral features are reproducible and are called statistical fine structure (SFS). When the concentration is dropped down to a ratio of one guest molecule per 10^{12} host molecules, the spectra of single absorbers can be resolved. See the lowest part of Fig. 2.

2.1 Fundamentals of SMS

Energy levels of a single molecule in solids (Jablonskii diagram)

The energy level scheme for an organic single molecule in a solid (a so-called Jablonskii-diagram) is shown in Fig. 3. The lowest electronic energy levels are two singlets S_0 and S_1 (left side of the picture), and a triplet T_1 (right side of the picture). S_0, S_1 and T_1 are electronic states, each of which includes correspondingly sets of vibrational states υ, υ′ and υ″ (see Fig. 3). The transition of the molecule from the ground state S_0 to the lowest excited state S_1 can be induced by laser light. This can be a purely electronic transition, which does not involve any molecular vibration (see ν_{00} in Fig. 3). It also can be a vibronic transition ν which additionally involves the excitation of molecular vibrations. In solid state matrices all molecular vibrations relax into the vibrational ground state of the respective electronic state through the creation of phonons on a picosecond timescale. This is called vibrational relaxation (VR). The non-radiative transition from S_1 to S_0 is called internal conversion (IC), because the transition occurs

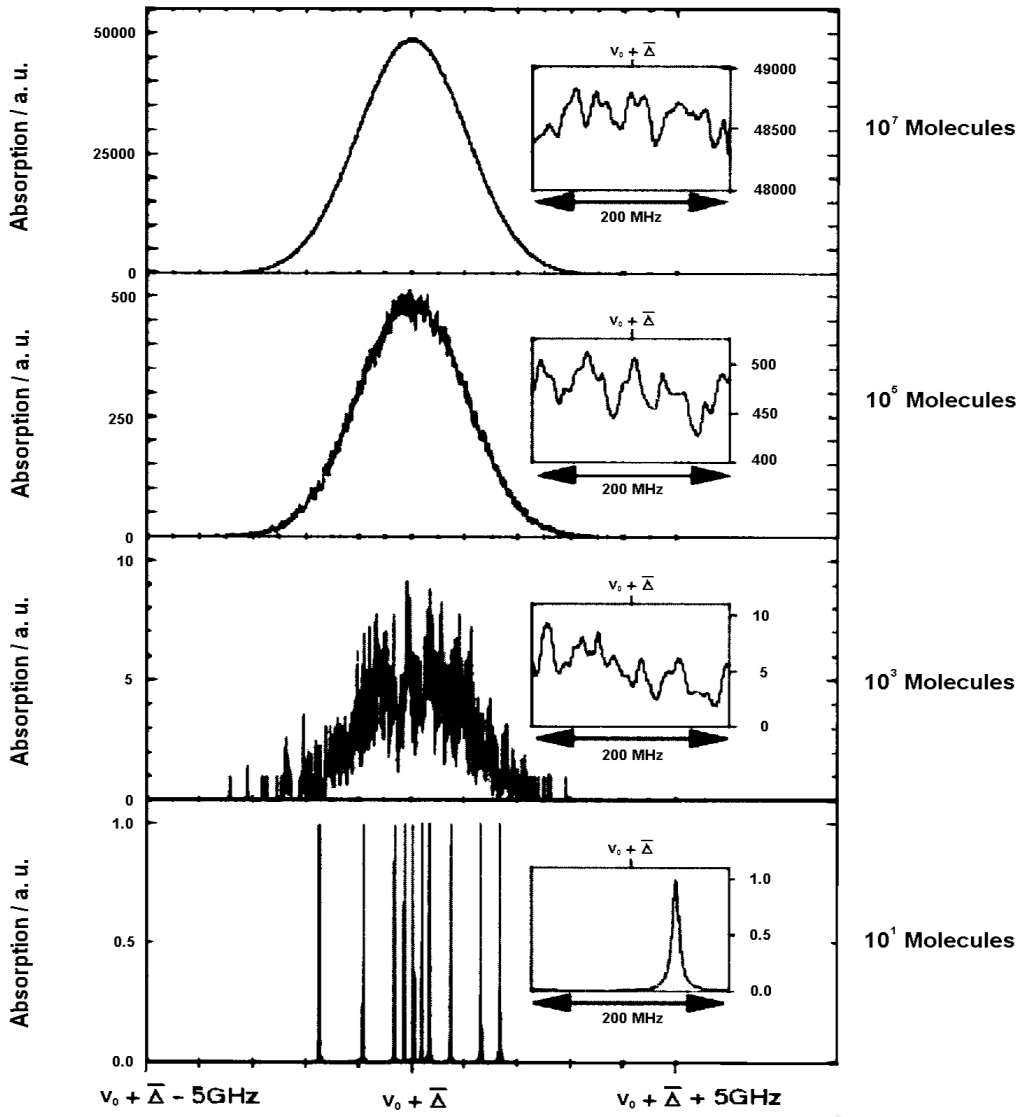

Fig. 2. Simulated inhomogeneous broadening: from broad inhomogeneous line down to single molecule spectra.

between states with the same spin. Vibronic transitions (S_0, $\upsilon = 0 \rightarrow S_1$, $\upsilon' = n$) are studied in the work of Nonn et al.[4] After a molecule has been excited to S_1 manifold, there are several pathways to relax to S_0, $\upsilon = 0$. First of all, the radiative transitions to one of the vibrational sublevels of S_0 - the fluorescence, normally detected in single molecule spectroscopy. In single-molecule experiments only the Stokes-shifted fluorescence is detected. The total radiative decay rate 2γ for terrylene molecules is typically 230×10^6 rad/s. A competing process to radiative transition is the nonradiative transition to the triplet state T_1 via ISC with probability of about 10^{-3} (this will vary from system to system). The transition between states with different spins, for instance $S_1 \rightarrow T_1$, is referred to as inter-system crossing (ISC). Radiative relaxation from T_1 to S_0 leads to the emission of the so-called phosphorescence. Transitions between the singlet and triplet manifold are spin-forbidden. They require spin-orbit coupling which is weak in hydrocarbons. Therefore the triplet state has a very long lifetime. The lifetime of the first excited singlet state S_1 is in the order of nanoseconds, while for triplet states the lifetime ranges from micro- to milliseconds. Intensively fluorescent molecule spend almost no time in the triplet state. Good candidates for single molecule spectroscopy therefore must fulfill the requirement that $k_{ST}/2\gamma$ and k_{ST}/k_{TS} are small. For instance, for terrylene molecule is typically $k_{ST}/2\gamma = 10^{-5}$ and $k_{ST}/k_{TS} = 0.27$.

Zero-phonon lines (ZPL)

The transition probability of a guest molecule in a host matrix depends on the coordinates of the surrounding atoms and is a function of the density and of the frequency of the vibrational states of the solid. Crystal lattice vibrations (phonons) are part of the ground state wave function. The phonon state population depends strongly on the temperature of the crystal, which in turn makes the absorption spectrum of the sample strongly dependent on the temperature. At room temperatures, the thermal motion has energy of about $kT \sim 300$

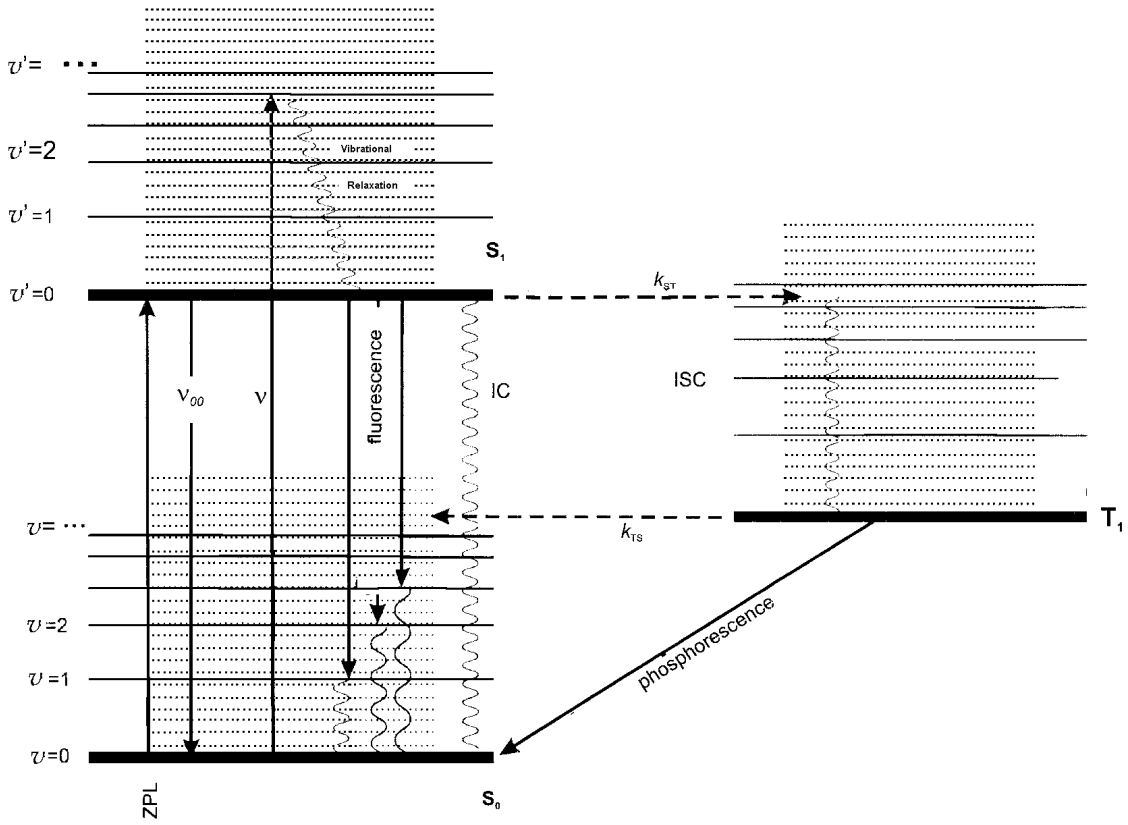

Fig. 3. Scheme representing the lowest energy levels of an organic single molecule embedded into a solid (Jablonskii diagram). Sets of υ-levels represent vibrational levels, and lighter drawn multiple lines are energy levels of the host's phonons. The radiative transitions are shown with solid lines, inter-system crossing (ISC) transitions with broken lines and internal conversion (IC) with waved lines. ν – frequency of the absorbed laser light, ν_{00} – frequency of the purely electronic transition with no phonons created (zero-phonon line), k_{ST} and k_{TS} are the rates of the singlet-triplet and triplet-singlet transitions.

cm^{-1} which is enough to excite a wealth of phonons, and the spectrum of the whole sample is tens to hundreds of cm^{-1} broad. With a decrease in temperature, the number of phonons is decreased. Thus, there appears a probability for electronic transitions without phonons involved, such are called zero phonon transitions, and the corresponding lines in spectra are called zero phonon lines (ZPL) (see Fig. 3). The lower the temperature, the narrower and more intense are the ZPL. The width of the ZPL is given by the inverse value of the excited state's lifetime. The study of ZPLs of single terrylene molecules in polyethylene at $T_0 = 30$ mK which is the lowest temperature so far was reported in the work of Donley et al.[5] The important property of ZPL's is that they provide characteristics of individual impurity molecules, which are defined by a molecule's environment (see Fig. 1). While the peak count rate of the lines reaches almost 10000 counts/s the background signal remains below 10 counts/s. This means that single molecules can be detected with a signal-to-background ratio of almost 1000.[6]

Lorentzian lineshape

The analytical expression describing the absorption lineshape of a single molecule can be obtained by solving time-dependent Schrödinger equations, leading to a system of Bloch equations.[7] For a two-level system shown in Fig. 3, the Bloch equations are:

$$\dot{\rho}_{11} = 2\gamma\rho_{22} + i\frac{\Omega_R}{2}(\rho_{21} - \rho_{12}) \quad (1)$$

$$\dot{\rho}_{22} = -2\gamma\rho_{11} - i\frac{\Omega_R}{2}(\rho_{21} - \rho_{12}) \quad (2)$$

$$\dot{\rho}_{12} = -i(\omega - \omega_0)\rho_{12} + i\frac{\Omega_R}{2}(\rho_{22} - \rho_{11}) - \gamma\rho_{12} \quad (3)$$

where γ is the radiative decay constant, Ω_R is the Rabi frequency $\Omega_R = \vec{d}_{12}\cdot\vec{E}_L/\hbar$, $\vec{d}_{12}$ is the transition moment of the molecule, $\vec{E}_L$ is the laser field, ω is the laser frequency, and ω_0 is the resonance transition frequency of the molecule.

The steady state solution of the Bloch equation ($\dot{\rho}_{11} = \dot{\rho}_{22} = 0$) gives us the rate of the spontaneous emission:

$$R = 2\gamma\rho_{22} = \frac{\Omega_R^2/4}{(\omega - \omega_0)^2 + \gamma^2 + 4\Omega_R^2/2} \quad (4)$$

According to Eq. 4, the spontaneous emission rate R has a Lorentzian lineshape with full width at the half maxima (FWHM) equal to half of the radiative decay rate (reciprocal to the lifetime of the excited state). Fig. 8 shows a typical single molecule spectrum recorded experimentally, with a width of about 8.9 MHz. The lifetimes of the excited state of individual molecules are different due to the local environment of the molecules. Fig. 7 shows the histograms of the linewidths of 54 perylene molecules in *n*-nonane. The lifetime limit estimated from the histogram is around 7.4 ns (136 MHz), while the maximum of the distribution is at about 20 ns (50 MHz). In most of the experiments, the average FWHM is less than several hundred MHz.

A more detailed theoretical and experimental analysis of the lineshape, leading to a slight deviation from Lorentzian line, is given in the work of Nonn.[6]

Absorption cross-section (ACS)

ACS represents the effective area that a molecule has to capture a photon. The radiative peak absorption cross-section (PACS) of a free atom is:[8]

$$\sigma_r = \frac{\lambda^2}{2\pi} \quad (5)$$

where λ is the vacuum transition wavelength at the absorption maximum. The peak absorption cross-section of a ZPL is reduced by the Debye-Waller factor $\alpha_{DW}(T)$ and by non-radiative and dephasing processes, as compared to the free atom case:

$$\sigma(T) = \alpha_{DW}(T)\frac{\gamma_{rad}}{\gamma_{hom}(T)}\beta(\theta)\frac{\sigma_r}{n^2} \quad (6)$$

where the factor $\beta(\theta)$ takes the linear polarization of the excitation light into account, with $\beta(\theta) = 3\cos^2\theta$, θ being the angle between the electric vector of the excitation light and the direction of the transition moment of the molecule, n is refractive index of the matrix.[9-11] A rough estimate for terrylene in *n*-hexadecane ($\alpha_{DW} = 0.5$, $\beta = 0.5$, $n = 1$, $\lambda = 572$) gives a PACS $\sigma(T) \approx 2.2 \times 10^{-10}$ cm^2, which is five orders of magnitude larger than geometrical ACS of terrylene 9×10^{-15} cm^2.

Basic SMS setup

A general experimental scheme for single molecule detection at low temperatures is shown in Fig. 4. The sample is a transparent solid (also called host) doped with dye molecules (called guests or impurities). The sample is inserted into a cryostat and cooled with liquid helium down to ≈ 2 K. The SMS experiments are performed at low temperatures (~ K), because at low temperatures the spectral lines are narrow and can be resolved with a tunable narrow-band laser beam ($\Delta\nu \approx$ 1 MHz). For a terrylene molecule in a naphthalene matrix, the linewidth increases from about 45 MHz at 30 mK to 80 MHz at 2.2 K.[12] At higher (or room) temperature, the individual molecules still can be detected if the concentration is low enough, but the spectral information will be lost. When the laser frequency is in resonance with the frequency of a guest molecule transition from the ground state S_0 to the first excited state S_1, the molecule absorbs $S_0 \rightarrow S_1$ and emits a photon $S_1 \rightarrow S_0$. Emitted photons are registered with a sensitive

detector. To distinguish the guest molecule fluorescence from Rayleigh scattering from the matrix, filters in front of the detector are used.

Spatial and spectral selection of a single molecule

The concept of single molecule selection is shown in Fig. 5. The way down to the detection of only one molecule begins with spatial selection. For low-temperature single molecule spectroscopy the impurity concentration in the sample volume should be about 10^{-7} M. The reduction of the sample volume (to a few hundreds μm^3) is done by taking the sample in the form of a thin, 1 μm, layer (a film for polymer matrices and a drop between two glass plates for liquid samples). Also, the laser beam is focused into a tiny spot (100 μm in diameter) on the sample. Thus, in the detection volume there will be about 10^4 dye molecules among 10^{12} solvent molecules. The next step – spectral selection, is based on the

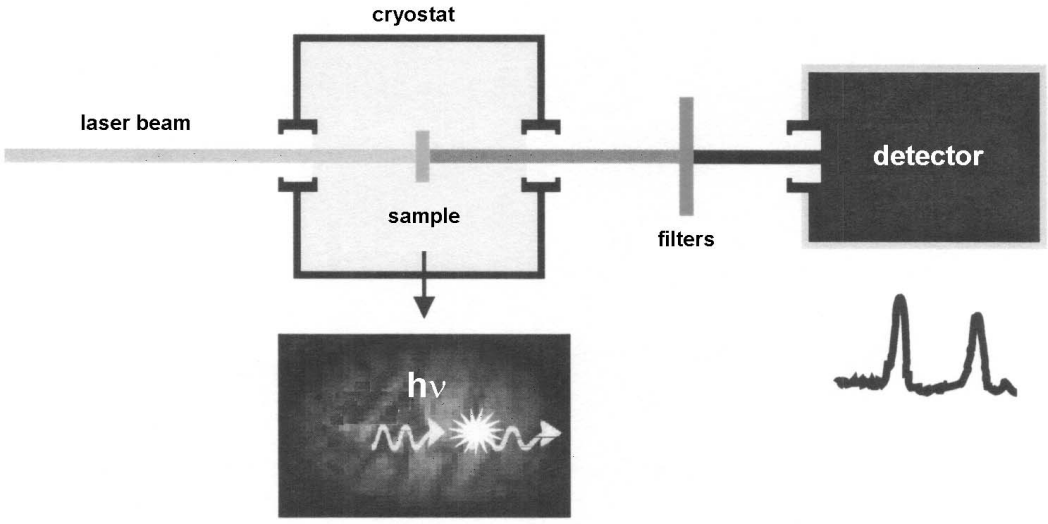

Fig. 4. General scheme of a low-temperature single molecule spectroscopy experiment.

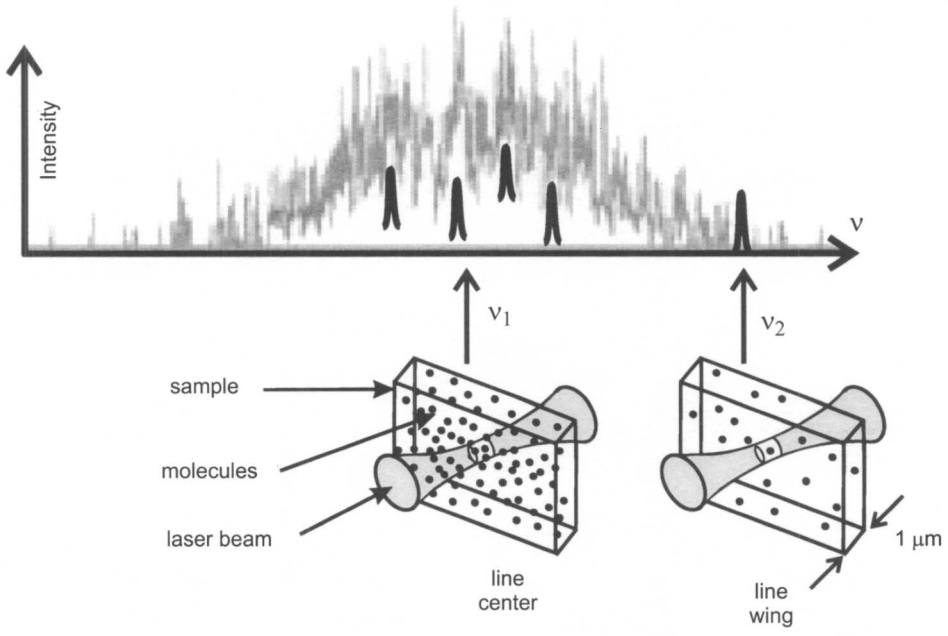

Fig. 5. An illustration of spatial selectivity by focusing the laser beam into a tiny spot (about 100 μm in diameter) and spectral selectivity by scanning with a laser over the wings of the inhomogeneously broadened line.

fact that the entire sample spectrum consists of single absorber lines which are 10^3–10^4 times narrower than the whole spectrum. By scanning over the wings of the inhomogeneously broadened line (where the single absorbers can be resolved) with the narrow-band laser, we can spectrally select one guest molecule out of 10^{12} matrix molecules (this ratio corresponds to a single letter in the 20-volume Oxford English Dictionary).

Figure 6 shows the fluorescence excitation spectra of a very low concentration sample of pentacene molecules in *p*-terphenyl at 1.8 K. The total frequency scan range shown is 10 cm^{-1}. Each of the peaks represents a single molecule, allowing approximately 450 molecules to be distinguished.

2.2 SMS experimental setup

In this section we discuss important parts of a low temperature single molecule experiment: light sources, cryostat, sample holding, detection system and optical filtering. One of the experimental setups which embodies these priciples is shown in Fig. 9.[13]

Light sources

To probe individual absorbers spectral lines with a typi-

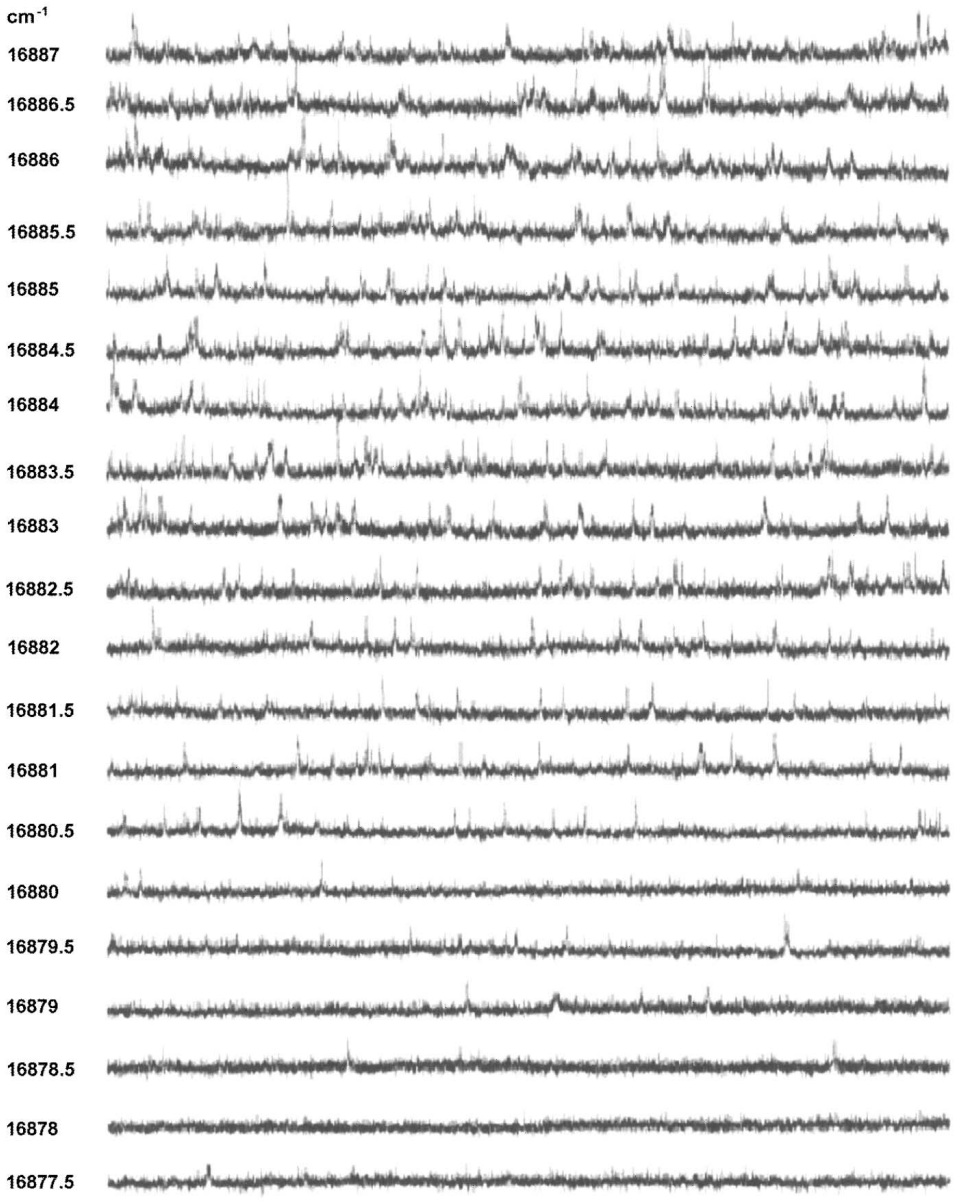

Fig. 6. Spectra of 450 single molecules. Measured by Frank Guettler and Marco Pirotta (using Autoscan laser). Sample was pentacene in *p*-terphenyl.[81]

cal width of a few MHz, a narrow-band detunable laser should be employed. For instance, to excite single terrylene molecules, whose excitation wavelength is about 572-578 nm, a single-mode dye laser (Coherent, model CR 599-21) with Rhodamine 6G (Radiant dyes) pumped by Argon Ion laser (Coherent, Innova 310) can be used. For experiments on perylene molecules, whose frequency of excitation is about 450 nm, a tunable blue laser light is required. This light can be generated by frequency doubling the IR output of argon ion laser pumped with a single-mode Ti:sapphire laser (Coherent 899-29) using an external cavity (wavetrain, LAS GmbH).[14] The laser provides an output power of about several tens of mW. Before the laser beam interacts with the sample, it should go through an interference filter to reject the direct light from the pump laser. An optical fiber can be employed to improve the beam profile and a half-wave plate can be placed in the laser beam path to rotate the polarization for the minimal angle between the molecular transition dipole moment and the polarization. To balance intensity changes during a frequency scan, the laser intensity has to be stabilized by a power stabilizer, for instance by one which uses a Pockels cell (Cambridge research, model LS100).[14] The laser

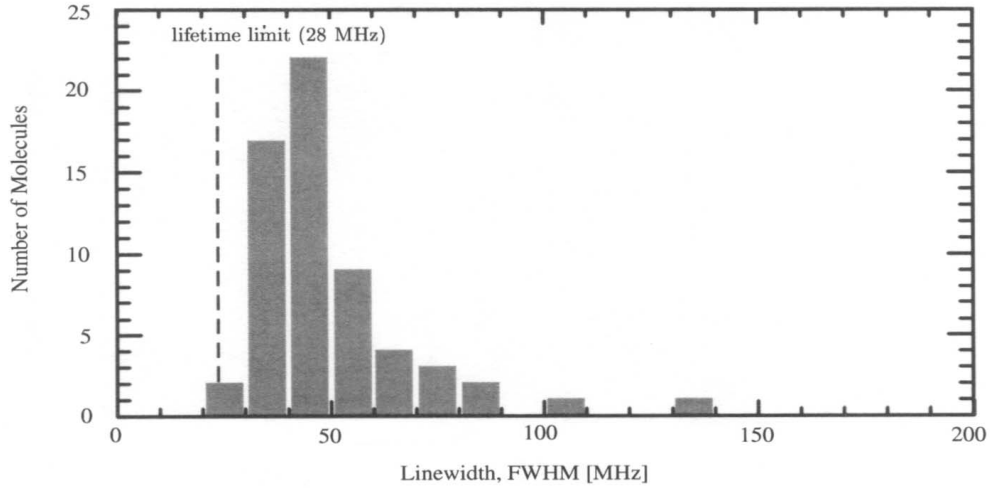

Fig. 7. Distribution of linewidth of 54 molecules in different perylene/*n*-nonane samples at 1.7 K. The maximum value of the FWHM is at 136 MHz, the lower cut-off is 28 MHz.[13]

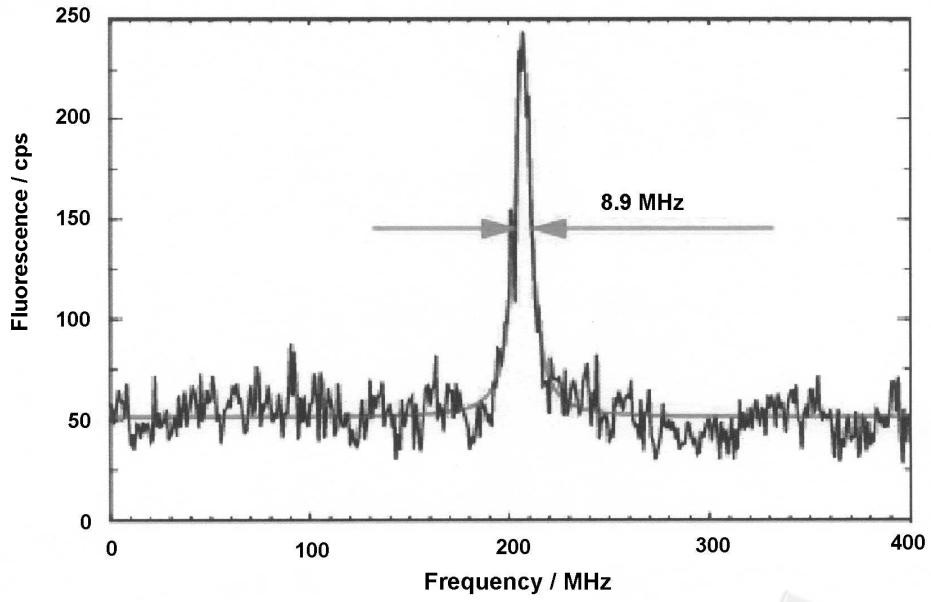

Fig. 8. A typical spectrum of a single molecule.

light should be focused to a tiny spot onto the sample, in order to fulfill the spatial selectivity requirement, described in the previous section. The focusing can be done by placing an achromat lens in front of the cryostat window, at a distance corresponding to the focal length of the lens.

Cryostat

Another important component of a low-temperature experiment is the cryostat. Gas-flow cryostat (Janis SVT 200) can be used for works with samples in liquid helium as well as in a gas-flow regime.[15,16] The core of the cryostat is the sample chamber, which is surrounded by the liquid helium chamber and by the nitrogen chamber. Layers of vacuum isolate the liquids from other chambers and from the environment. Once having a good sample, one can keep it for weeks in a crystal state by re-filling the cryostat with liquid nitrogen. Oxford cryostats have a large enough helium reservoir to operate below the λ-point for more than 24 hours.[4] A special type of home built Oxford cryostat provides very low temperatures down to 30 mK and single molecule spectra detected with such a cryostat at 30 mK are described in the PhD thesis of Donley.[17]

Sample holding

A typical way to hold a sample in a cryostat is to make a so-called "sample sandwich'' and fix it onto a sample holder (see Fig. 10). The sample can simply be placed between two thin pieces of glass or filled into a thin cuvette. Different modifications of this arrangement (in the cases of Stark and pressure effect experiments) will be discussed later in the corresponding sections.

Microscope objectives

In order to collect the SM fluorescence coming out of the sample at a very wide angle, a microscope objective (for instance, Newport M-60, NA = 0.85) should be placed right behind the sample (see Fig. 10). When immersed in superfluid helium, the objective's resolution deteriorates due to a change in focal length caused by the slightly different index of refraction of the space-filling superfluid helium between the lenses as compared to air. Refocusing at the liguid helium temperature is performed by moving the objective along the optical axis using a stepper motor (for instance, Princeton Research vacuum stepper motor, home-rebuilt for working in helium).[16,18]

Filters

There are some typical filters almost used in every SMS setup: interference filter (Oriel, 580FS10-50 for λ = 574 nm) to clean the excitation laser light before it enters the sample,

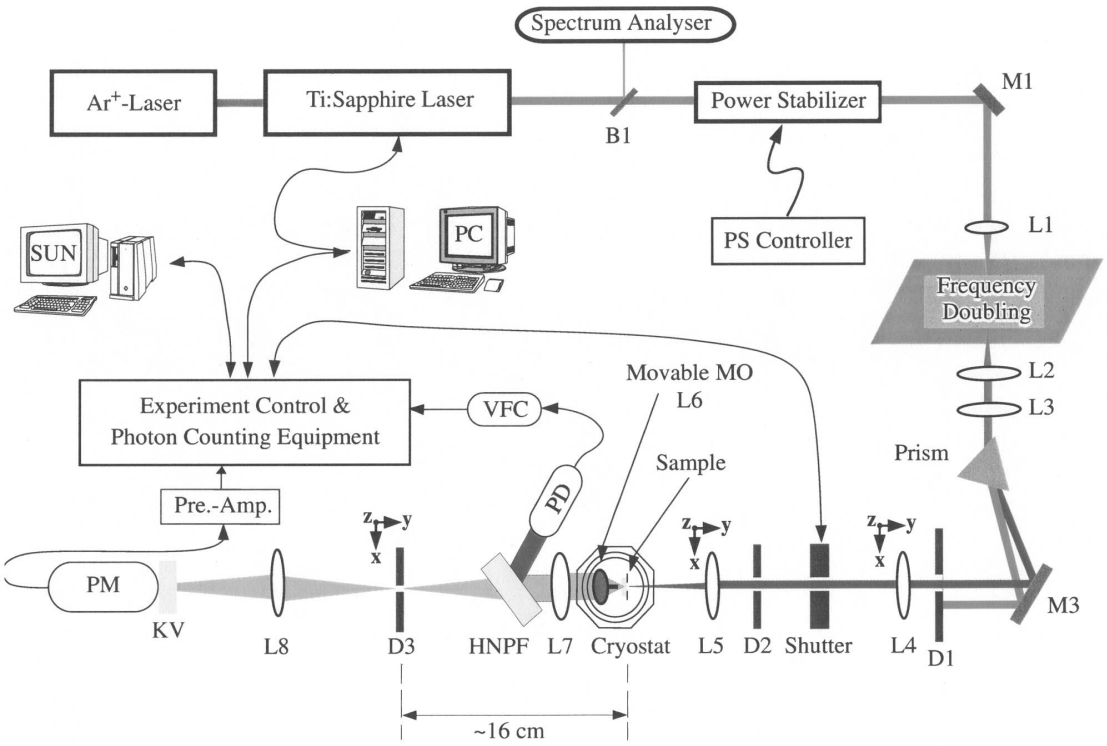

Fig. 9. An example of a low-temperature single molecule setup. M denotes mirrors, L are lenses, D are diaphragms, B1 is a beamsplitter. For details see PhD thesis of Marco Pirotta.[14]

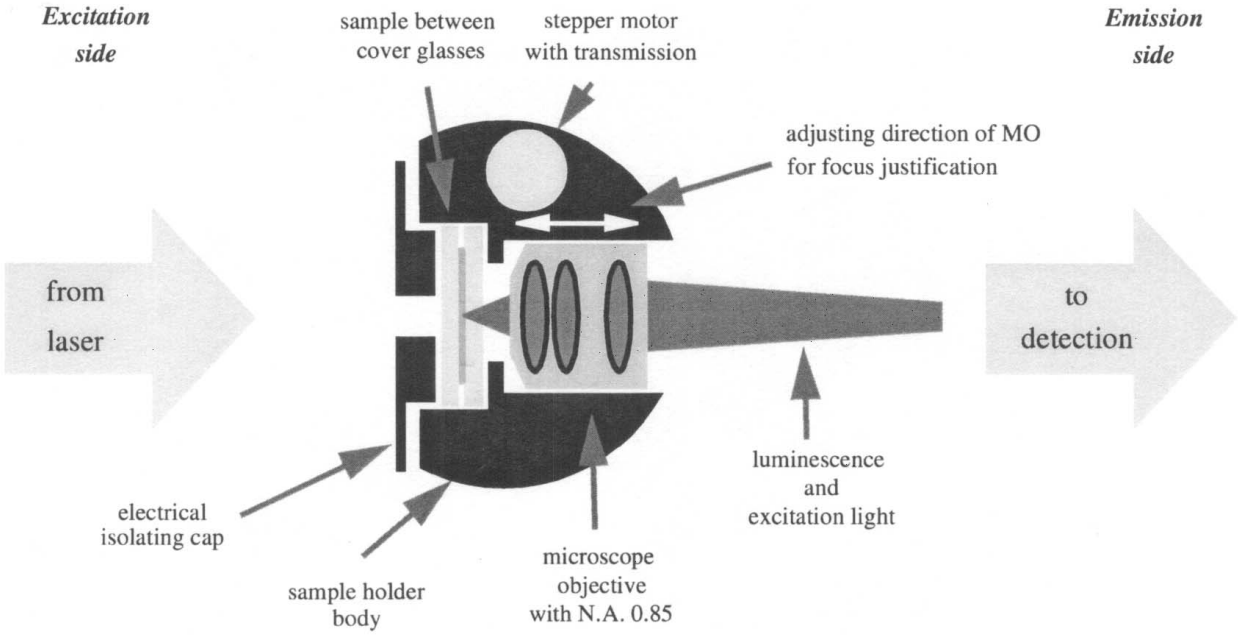

Fig. 10. Schematic drawing of the arrangement of sample and microscope objective in the sample holder body. The cap is fixing the sample "sandwich". The distance between the microscope objective and the sample is adjusted with a home-built stepper-motor while the sample-holder is immersed into the liquid helium at 1.7 K.[14]

notch filter in front of the detector to separate the fluorescence from the laser light, and sometimes a cut-off glass filter to reject excessive stray light. For instance, the scheme shown in Fig. 10 uses a holographic notch filter (HNPF, Kaiser Optical System, center rejection wavelength 574 nm) and cut-off filters (KV, Schott RG610). In some experiments, the optics with flat surfaces (filters or microscope objective) can be tilted to avoid interference fringes that increase the background signal.[6]

Detectors

The maximum total efficiency, C_{tot}, of detecting fluorescence photons is given by a combination of collection efficiencies and transmission factors:

$$C_{tot} = C_{max\ angle} T_{filters} T_{optics} C_{detector} \tag{7}$$

$C_{max\ angle}$ describes the maximum angle of light, from which light can be collected with the MO, and completely determined by the numerical aperture of the MO:

$$C_{max\ angle} = \frac{1}{4}\left\{1-\cos\left[\arcsin\left(\frac{n_{LHe}\mathrm{NA}}{n_{glass}}\right)\right]\right\} \tag{8}$$

for details of this formula see Ref. 14 and 19. For an MO with NA = 0.85, maximum angle is $C_{max\ angle} = 0.05$. Transmission efficiency of the notch filter is about 55%, giving us $T_{filters} =$ 0.55. The overall transmission through the optical parts, for instance, for the scheme shown in Fig. 9, consisting of 12 optical elements, is: $T_{optics} = 0.96^{2\times12} = 0.38$. The quantum efficiency of a PM varies between 10–20%. Thus, the maximal collection efficiency of the apparatus is:

$$C_{total} \sim 0.2\% \tag{9}$$

To detect single molecule fluorescence, such detectors as a sensitive CCD camera (Hamamatsu C2400-25 with image intensifier), photomultiplier (PM) (dry-ice cooled PM tube RCA, C31034) or avalanche photodiode (APD) can be used.

Samples

How many photons are needed to see a single molecule? Ideally, a guest molecule excited by laser light to resonate, circulates between its ground and first excited states and emits one photon every ~ 10^{-9}s. This means that there should be 10^9 photons emitted every second, which is more than enough to detect the molecule which requires 10^6 photons per second. The presence of a long living (up to a few ms) triplet state dramatically decreases the amount of emitted photons. Good guest candidates for single molecule spectroscopy should have a short living triplet state, which leads to the high emission rate of the molecule. Guest molecules should have a high absorption cross section. There also should not be no

emission from the host molecules. A resent overview on a guest-host system studied by SMS can be found in.[20]

Sample preparation

So-called Shpol'skii systems, used in low-temperature SMS, are obtained by simply dissolving a tiny amount of dye in liquid *n*-alkane. The crystals are formed under a fast cooling procedure.[15]

Naphthalene[16] or *p*-terphenyl[9] crystals doped with dye molecules are prepared in a sublimation tube, see Fig. 11. A tiny speck of terrylene and a mixture of the naphthalene isotopes become molten under magnetic stirring. The melt is filled into the glass tube, sealed with the cold finger and flushed with dry nitrogen gas for half an hour. Meanwhile, the polyethylene glycol bath is heated to 180 °C. Then, the glass tube is immersed into the heat bath so that the cold finger is about 1 cm above the level of the glycol surface and kept there for about 1 hour. During the sublimation, the tube is constantly flushed with dry nitrogen and the cold finger with water at 20°. Small crystal platelets (surface < 1 mm^2) are quickly formed at the top of the finger, larger crystal (surface > 1 mm^2) condense slowly at the upper part. After about one hour, the heating can be switched off and the crystals can be carefully collected from the cold finger and stored at -18 °C for several weeks.

The spin-coating technique is used to produce thin polymer films doped with dye molecules. The sample is a co-solution of a polymer, for instance 10% polymethylmetacrylate (PMMA) (10 mg/mL) and a dye (10^{-9} M) in toluene. A drop of the solution is put onto a spinning microscopic coverslip, which has been prelimiarily heated at about 300 °C for several hours in order to remove potential fluorescence contamination.

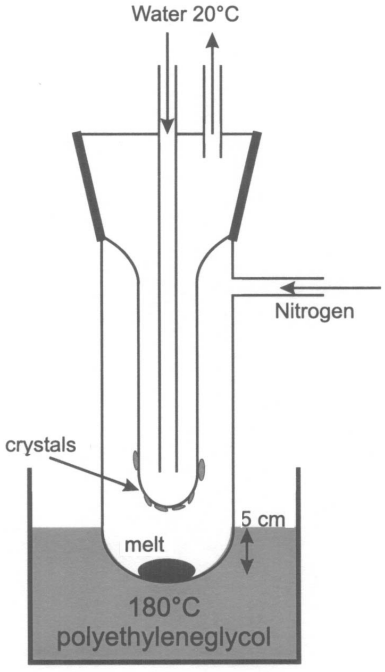

Fig. 11. Apparatus for the fabrication of naphthalene crystals doped with dye molecules.

Parallel spatial and spectral detection of many single molecules

Most of the low temperature techniques use wide-field illumination, when many molecules can be excited at a time by a 100-200 μm diameter laser spot. The spatial resolution of the system is then dominated by the optical resolution of the microscope. The advantages of such technique are twofolded. Firstly, the molecules in the illuminated area are excited and detected at the same time, so that we can be more certain that all of the molecules are studied under identical macroscopic conditions. Secondly, except for analyzing the property of an individual SM, the measured property of individual molecules can be easily averaged to bridge the SM regime to the bulk sample regime. A result of such an experiment is shown in Fig. 12. The picture shows a 3-D plot representing *spatial* intensity distribution of the fluorescence signal at a given excitation frequency. The three obvious peaks represent three SM. The three 2-D plots in the insets show the spectral dependencies of the three molecules, recorded while the laser frequency was scanned. Though, all three molecules have maxima of fluorescence almost at the same frequency (at the frequency where the spatial 3D plot was made), they have different spectral behaviour. Molecule γ even disappeared half way during the frequency scan, causing a sharp drop in the spectral line shape, indicating perhaps a chemical reaction which quenched the molecule.

Further details about single molecule experimental setups can be found in the literature.[6,9,14-16,21]

2.3 Low temperature single molecules experimental technigues

2.3.1 Fluorescence excitation spectra

The first detection of single molecules absorption lines was performed in an absorption experiment[22,23] with frequency modulation (FM) spectroscopy to eliminate low-frequency laser noise. One year later, Michel Orrit[24] proposed another technique for single molecule detection: fluorescence-excitation spectroscopy. Since then, most single molecule experiments at low-temperature have been performed using the fluorescence excitation technique. In this technique, the wavelength of the excitation light is scanned, and the total Stokes shifted fluorescence as a function of the excitation frequency is recorded (see Fig. 3). Typical setup

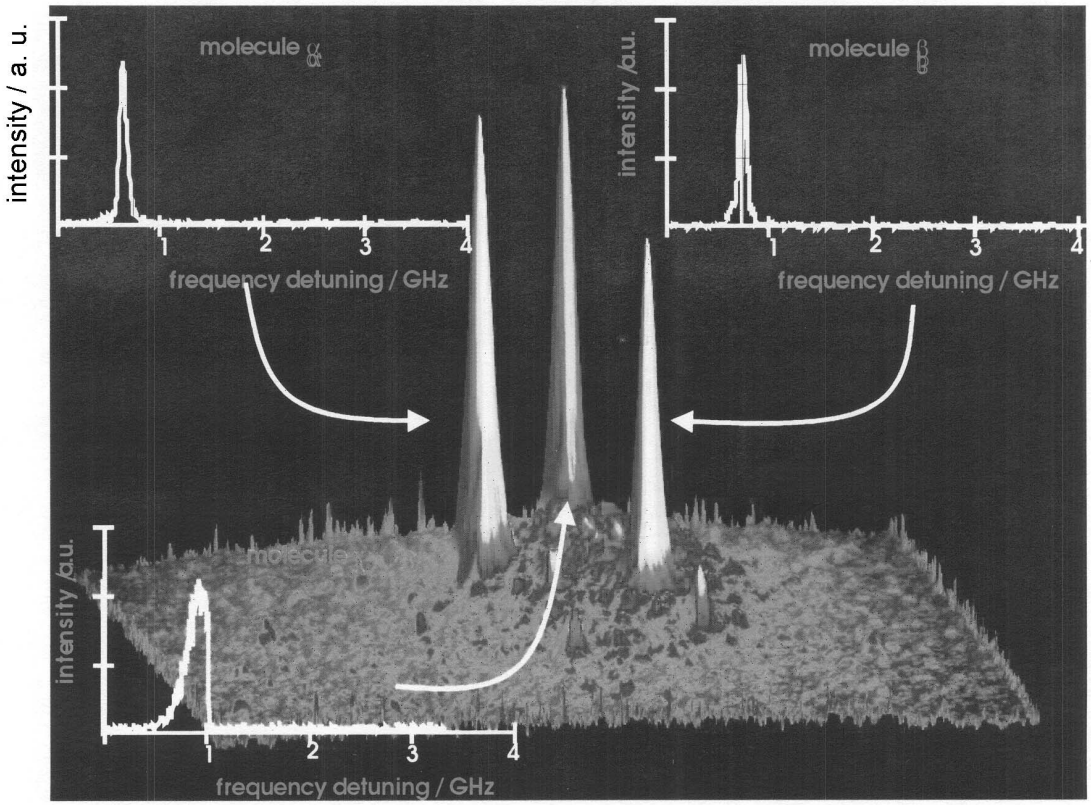

Fig. 12. Fluorescence image of DBATT (dibenzanthanthrene) single molecules in Xe crystal.[36]

for fluorescence excitation study has already been discussed in the previous section (see Fig. 9). The next sections are dedicated to the special techniques developed in Wild's group to resolve vibronic, emission and absorption spectra of single molecules.

2.3.2 Vibronic excitation spectra

The purely electronic transition line corresponds to a transition of the chromophore from the ground to the electronic excited state: S_0, $\nu = 0 \rightarrow S_1$, $\nu' = 0$, where molecular vibrations are not excited. However, it is also possible to study the transitions of the chromophore from the ground state to the electronic excited state S_0, $\nu = 0 \rightarrow S_1$, $\nu' = n$ or the so-called vibronic lines, which involve the excitation of a local phonon at the same time.[4,6] Since the lifetime of the local phonon lies in the range of several picoseconds, the width of vibronic lines at liquid helium temperature is about 1 cm^{-1}. Figure 13 shows two regions of the fluorescence excitation spectrum of terrylene in naphthalene. The left part is characterized by sharp purely electronic absorption lines of individual terrylene molecules. The right part is dominated by two broad almost structureless bands ν_1 and ν_2 corresponding two vibronic transitions. To extract the individual vibronic spectra from the broad bands, a two-laser scheme was proposed[6] (see Fig. 14). The principle of the technique is as follows: one laser is pumping at a single molecule resonance frequency and the other laser's frequency is scanned over. The transition of the molecule in resonance with the pumping laser is saturated, and this molecule will not show up in the spectra (see Fig. 15). This technique demonstrates how it is possible to remove the contribution of individual molecules to excitation spectra. Figure 16 shows two spectra of the first vibronic band ν_1. One spectrum was recorded with laser I only, and the other spectrum was recorded with lasers I and II, with laser II in resonance with the purely electronic transition of a single molecule. The difference between the two spectra yields the single-molecule vibronic line as shown in Fig. 17.

2.3.3 Emission spectra

While most low temperature single molecule experiments employ fluorescence excitation technique, there is also the possibility to excite the molecule with a fixed frequency in the maximum of its absorption line and disperse the emitted fluorescence light by a monochromator. With this so-

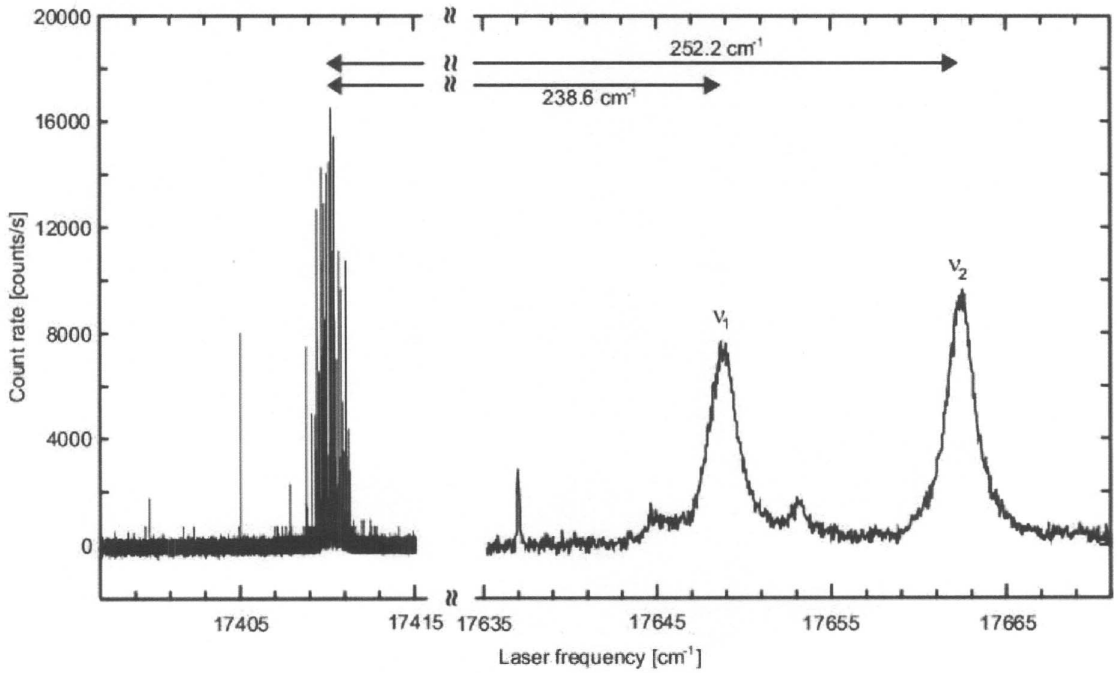

Fig. 13. Fluorescence excitation spectra of terrylene in naphthalene. To the left, narrow lines owing to the excitation of the purely electronic transition of individual molecules are visible. To the right, vibronic bands of two low frequency vibrations of terrylene appear.[6]

called spectral imaging technique, the vibrationally resolved fluorescence spectrum of a single molecule can be recorded. A vibrationally resolved fluorescence spectrum provides more information about a single molecule, which has been shown in several investigations.[25-30] Emission spectra on single terrylene molecules in naphthalene matrix were recorded by Hermann Bach in his PhD work.[16] For spectral imaging, the sample fluorescence is imaged onto the entrance slit of a 0.27 m imaging spectrometer (JOBIN YVON-SPEX 270M) equipped with a 1200 g/mm holographic grating and detected with a liquid-nitrogen-cooled CCD chip (1024 × 256 pixels, 27 μm pixel size, quantum efficiency 50%). In this configuration, the spectral resolution is about 3 cm^{-1} at detection wavelength near 600 nm with a 50 μm wide entrance slit and 75 nm spectral range can be covered by the chip. The dispersed emission spectra were calibrated in frequency using dye laser lines and the neon-emission lines from calibration lamps (PEN RAY). To record the emission spectrum of an ensemble of molecules, the entrance slit was 50 mm and the signal was integrated over the vertical dimension of the chip for one second. For spectral imaging of many single molecules in parallel, the entrance slit was opened to 2 mm and 1024 × 256 pixel images were recorded by accumulating the signal for 5 s. To locate the spatial position of the molecules, the spectrometer was used in two different configurations. First, the fluorescence light that passed the notch filter, which was dispersed by the grating into the first diffraction order, was recorded. Afterwards the total luminescence that was long-pass-filtered by the notch and the cut-off filters and reflected into the zeroth diffraction order was registered. In the first case, spectrally dispersed images – referred to as first-order images – are obtained and the horizontal axis of the CCD chip comprises a frequency and a spatial dimension. In the latter case, the CCD chip serves simply as a two-dimensional detector for the total luminescence of the sample and images referred to as zeroth order images are obtained. First and zeroth-order images are combined to yield the spectral image. The monitored sample area depends on the magnification of the objective and on the entrance slit and chip dimensions. For a slit width of 2 mm, a sample area of approximately 20 mm (horizontal) by 80 mm (vertical) was imaged onto the chip.

Figure 18(a) shows the emission spectrum of an ensemble of terrylene molecules in naphthalene d_8 recorded by integrating the dispersed fluorescence light that passed the notch filter and the 50 μm wide entrance slit along the vertical dimension of the CCD chip for 1 s.[16] The position of the vibrationless transition is given by the attenuated laser line that was subsequently recorded. All other peaks belong to transi-

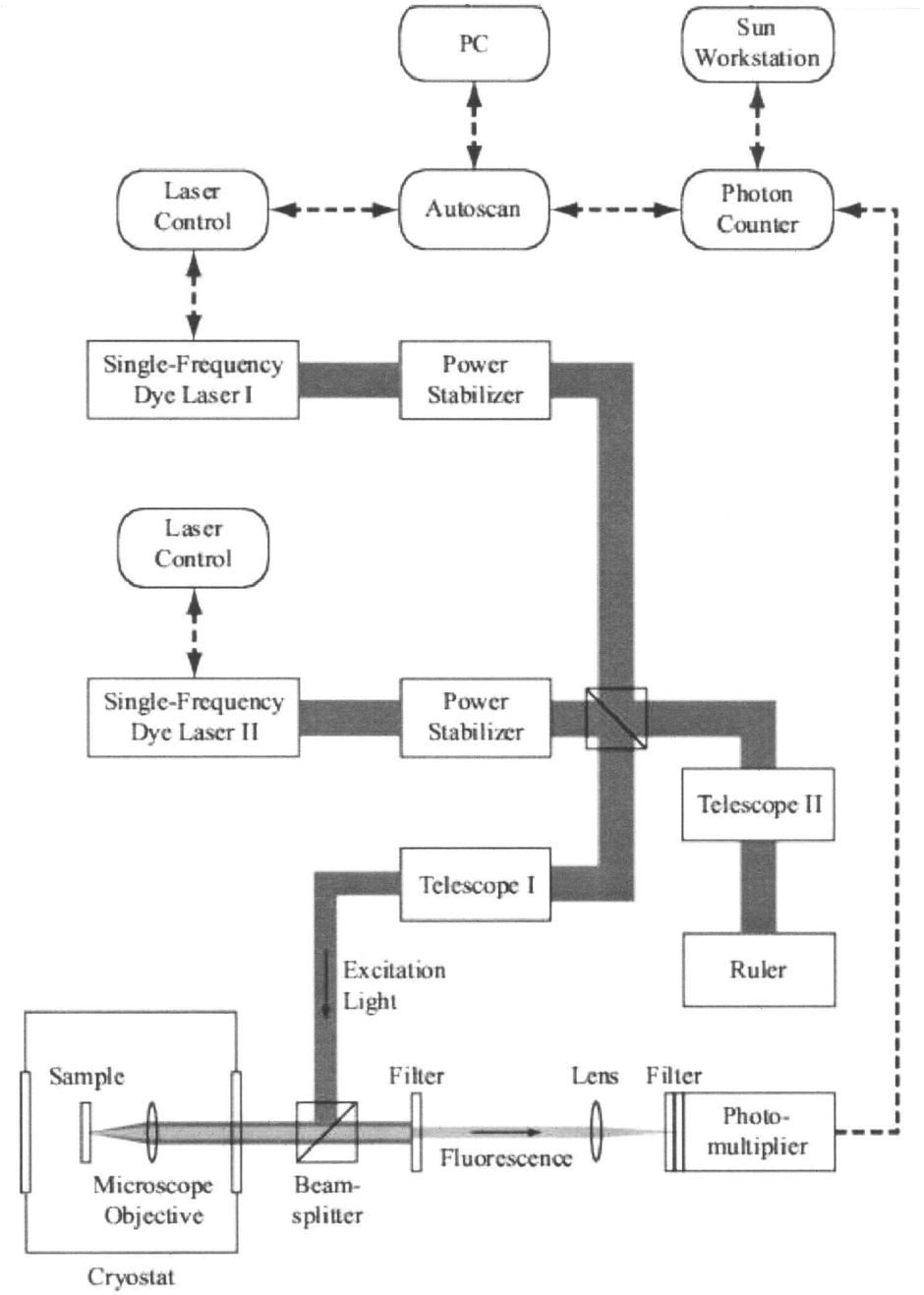

Fig. 14. Experimental setup for the observation of the vibronic transitions in single molecules. The frequency of laser I is scanned, laser II is used to remove the contribution of single molecules to the spectrum.[6]

tions from the vibrational ground state of the electronic first excited state to higher vibrational levels of the electronic ground state. The ground-state vibrational frequencies can be obtained by determining the spectral distance between the emission peaks and the frequency position of the laser line. Without integrating over the vertical chip dimension, the spectral image depicted in Fig. 18(b) is obtained by signal integration for 5 s. The dark colored vertical stripes correspond to fluorescence emission from molecules out of focus at the entrance slit. When the entrance slit is opened to 2 mm, the spectral image Fig. 18(c) is obtained by combining the zeroth order and the first order image. In the spectrally dispersed entrance slit image (first order image), fluorescence emission peak sequences of single molecules focused at different spa-

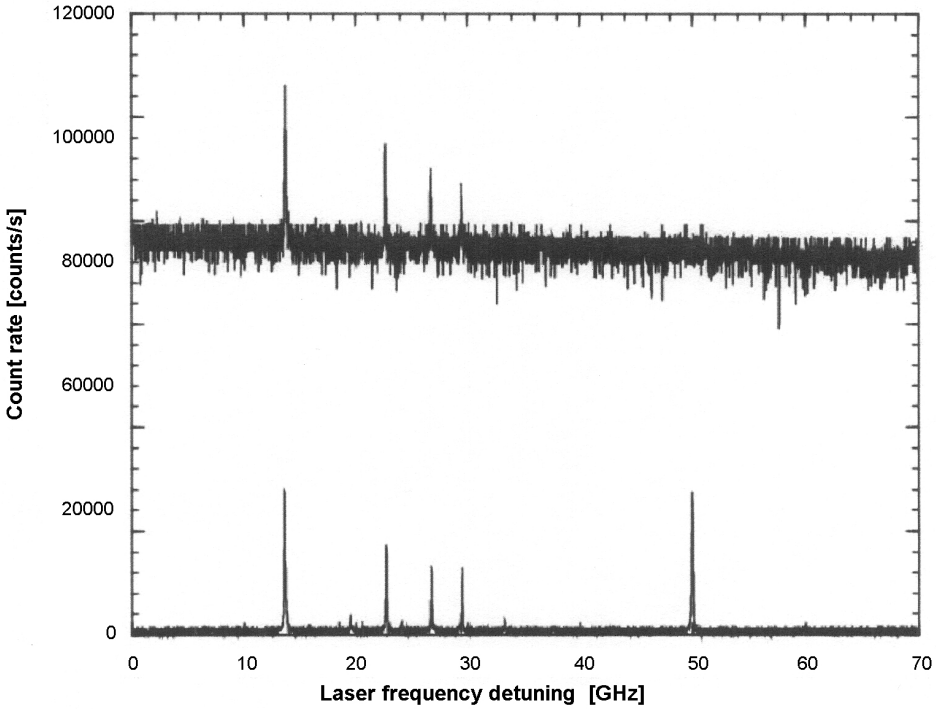

Fig. 15. An illustration of removing a single molecule from spectra by using two-laser technique. The lower spectra is recorded with one laser only (laser I in Fig. 14). Five peaks correspond to five single molecules. The upper spectra has been taken over the same molecules, when the second laser is tuned into the 5-th molecule's resonance frequency. Obviously, the peak from the 5-th molecule disappeared.[6]

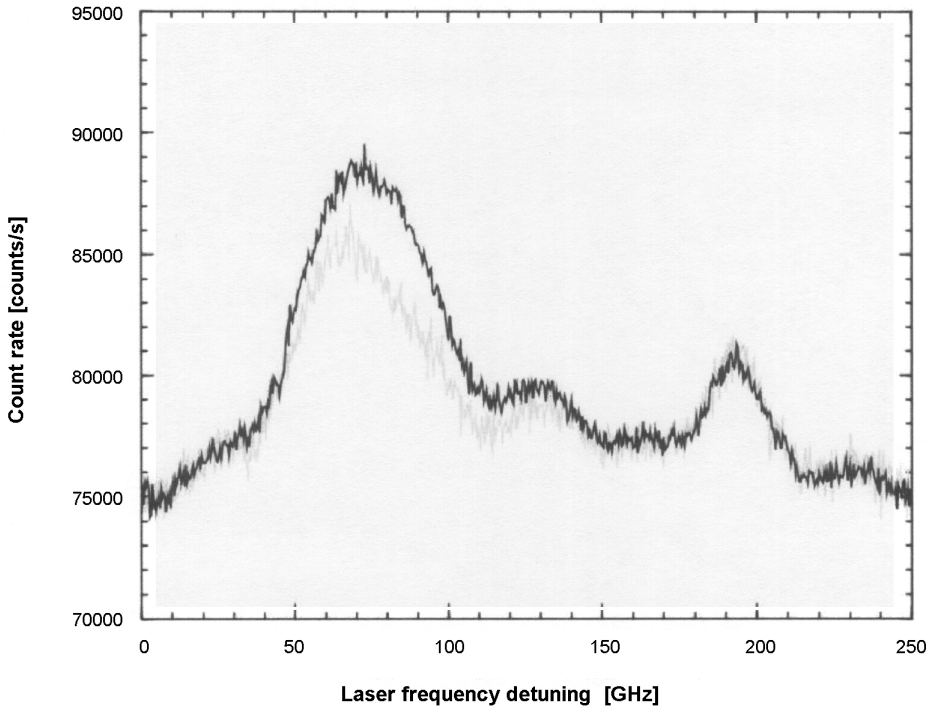

Fig. 16. Two spectra of the ν_1 vibronic band. The black spectrum is recorded with one laser, and the grey spectrum is recorded with two lasers. One molecule is missing in the grey spectrum.[6]

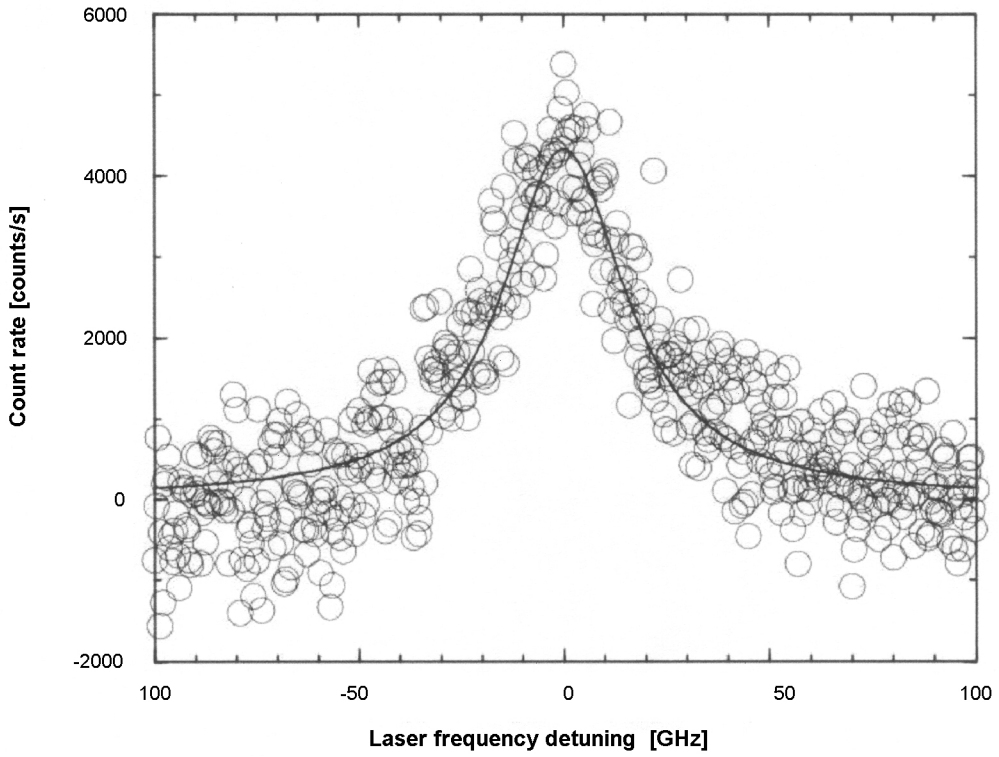

Fig. 17. Result of subtraction of the two spectra in Fig. 16. Fitting a Lorentzian to the data yields a linewidth of 37(2) GHz and a peak count rate of 4530(160) counts/s.[6]

tial locations in the entrance slit plane emerge on top of the background from molecules that are out of focus. The peak sequences are horizontally shifted relative to each other reflecting the different spatial locations of the focused molecule images in the entrance slit plate. A fluorescence emission spectrum is obtained from the data by integrating the fluorescence signal in a pixel array centered on single molecule emission peaks followed by background subtraction.

2.3.4 Absorption spectra

The first spectroscopic investigation of single molecules was an absorption measurement which used a complicated double-modulation scheme.[22,23] It was based upon optical frequency-modulation spectroscopy (FMS)[31] with modulation frequencies ν_m between 51 and 91 MHz to eliminate low-frequency laser noise. FMS experiments are affected by residual amplitude modulation (RAM) which produces spurious background signals owing to unavoidable imbalances between the amplitudes of the two laser side-bands.[32] Hence, a secondary modulation had to be used to eliminate the RAM. Two different techniques were applied, namely, AC Stark modulation (modulation frequency f_m = 2-5 kHz) and ultrasonic modulation (f_m = 2-5 MHz). Both techniques cause a periodic shift of the molecular absorption frequency. With both methods, single-molecule spectra could be recorded but the signal-to-noise ratio (SNR) was only about two or three.[22,23] Shortly afterwards, the first fluorescence-excitation experiment on single molecules was performed which provided a much better SNR with a simpler set-up.[24] Therefore, all subsequent experiments used the fluorescence excitation scheme. Although the absorption experiment reported in the present work repeats the first single molecule experiments,[22] it employs a less sophisticated electronic scheme.[33]

The experimental set-up is schematically depicted in Fig. 20. The optical scheme is analogous to a standard SMS scheme described in Sec. 2.2 with the following differences: the microscope objective is placed in front of the sample to focus the laser beam on a *single molecule*; no filters are used in front of the detector. For experimental details see the PhD. work of Latychevskaia.[18]

When a radio-frequency (RF) electric field is applied to a single molecule its absorption line moves in the spectral domain with the same frequency Ω_m. In the case of low modulation frequencies, the single molecule absorption line oscillates with the frequency of modulation Ω_m:

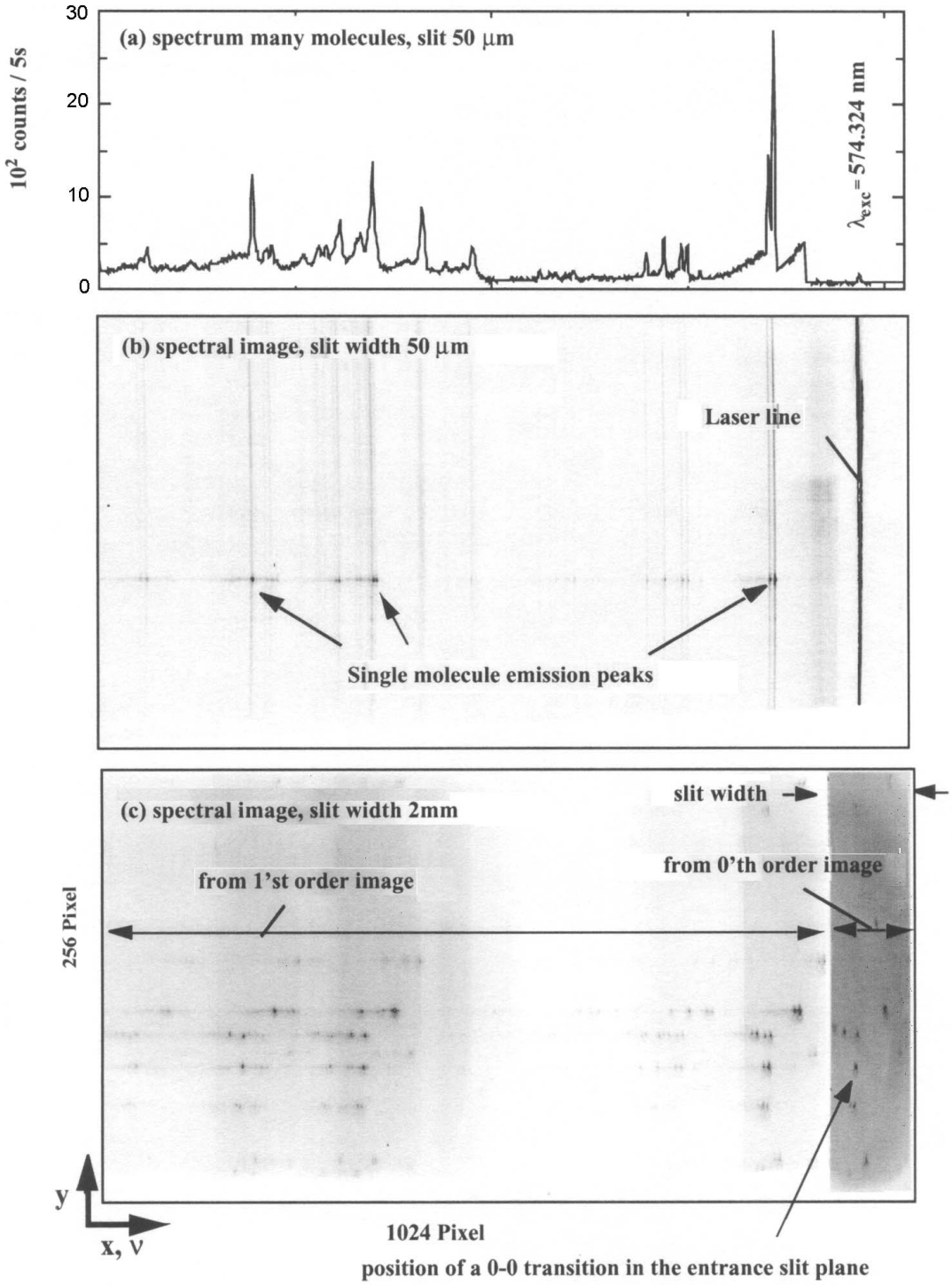

Fig. 18. (a) Fluorescence emission spectrum of an ensemble of terrylene molecules in naphthalene d_8. (b) Spectral image recorded with the spectrometer's entrance slit narrowed. Dark colors correspond to high fluorescence intensity. The emission spectrum of a single molecule focused in the entrance slit plane appears as a sequence of dark spots along the horizontal axis. The dark stripes belong to fluorescence from defocused molecules. (c) Spectral image comprising the spectrally dispersed image (first order image) and the image reflected in zeroth diffraction order recorded with the entrance slit opened (See Ref. 16 for details).

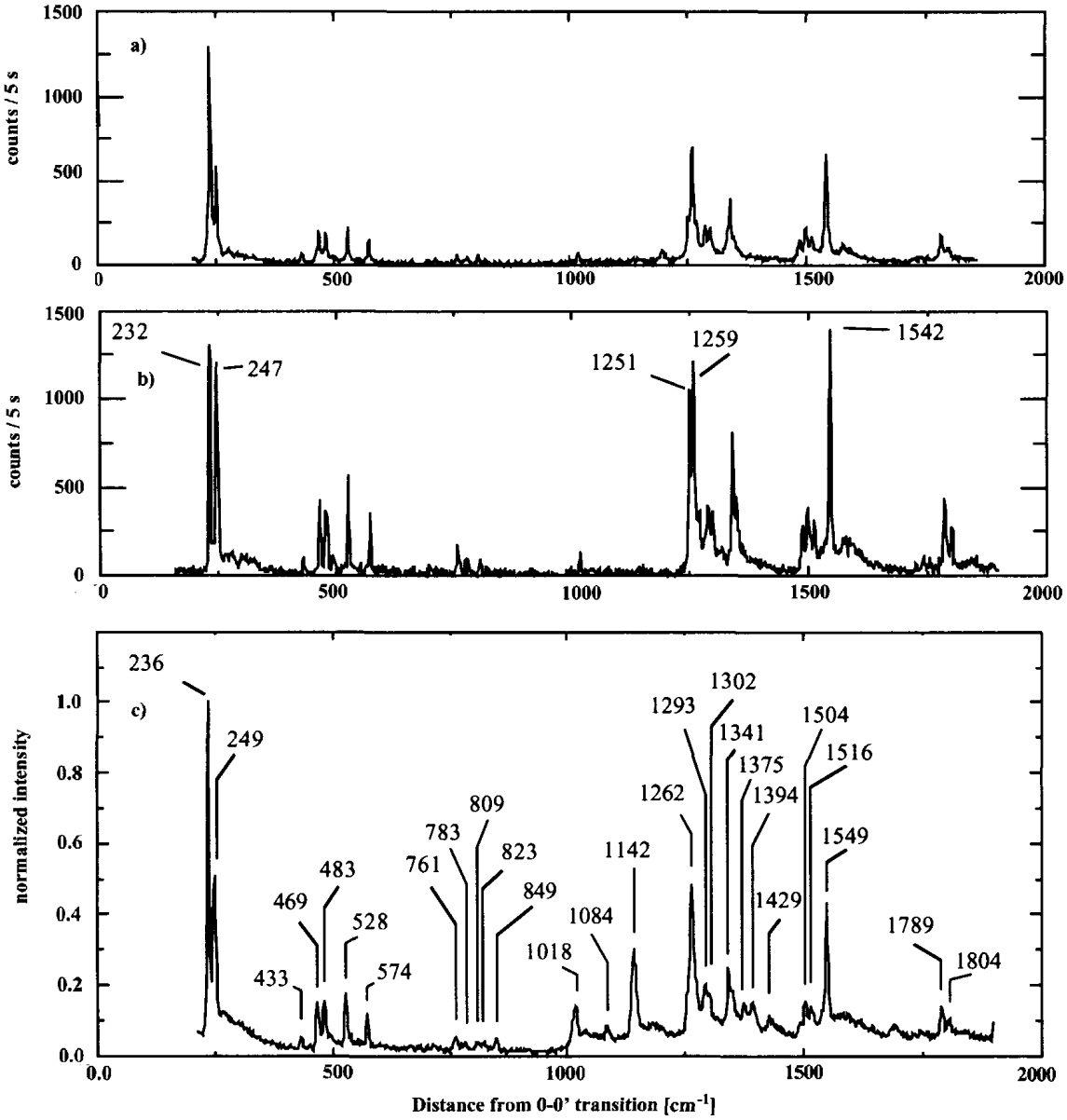

Fig. 19. Emission spectra of terrylene in naphthalene d_8. a) and b) are spectra of single terrylene molecules, c) is the ensemble emission spectrum with the vibrational frequencies assigned to the peaks.

$$G(\nu,t)=\frac{\gamma_{\text{hom}}}{(\nu-\nu_0-\nu_E^{\max}\cos(\Omega_m t+\phi_m))^2+\gamma_{\text{hom}}^2} \tag{10}$$

where $\nu_E^{\max}$ is the maximum frequency excursion owing to the linear Stark effect:

$$\nu_E^{\max}=\frac{1}{h}f_{\text{L}}\Delta\vec{\mu}_{\text{ind}}\cdot\vec{E}_{\text{ext},0} \tag{11}$$

γ_{hom} is the molecular homogeneously broadened linewidth, $\vec{E}_{\text{ext},0}$ is the amplitude of the RF field, $\Delta\vec{\mu}_{\text{ind}}$ is the difference of the induced dipole moments in the excited and the ground state of the molecule, f_{L} is the Lorentz factor determining the local electric field strength inside the solid matrix, h is Planck's constant, Ω_{m} is the modulation frequency and ϕ_{m} is the phase relative to the local oscillator (molecule).

The signal at the detector output consists of a DC component and a time-varying component proportional to the amplitude of the modulation of the transmitted light beam:

$\exp(-G(\nu, t))$.

$$\exp(-G(\nu,t)) \sim 1 - G(\nu,t) \tag{12}$$

To extract the DC component or to demodulate the photo-current signal, a mixer is used. Phase-sensitive demodulation of the photo-current signal in the mixer yields a line shape which is proportional to the derivative of the molecular absorption line (for sufficiently small modulation amplitudes):

$$\left\langle (-G(\nu,t)) \sin(\Omega_m t) \right\rangle \tag{13}$$

where $\langle\ \rangle$ represents the time average. This is analogous to the phase-sensitive ultrasonic modulation of hole spectra[34] and also to standard experiments in electron paramagnetic resonance (EPR).[35]

Figure 21 shows the absorption signal of a single terrylene molecule in *n*-hexadecane. The laser wavelength was 572.097 nm, the modulation frequency being 1 MHz. The laser frequency was scanned over 2 GHz range and then back in the reversed direction with the same rate. Hence, two copies of the absorption line appear in the plot. The line shape represents the derivative of a Lorentzian profile with equal amplitude above and below the baseline so that we can conclude that this molecule shows a linear Stark effect. The signals at ± 0.6 GHz have a slope of the opposite sign; hence, the corresponding molecule shows a Stark shift in the opposite direction.

2.3.5 Matrix isolation technique

Matrix isolation is a technique for trapping reactive species at very low temperatures, where a guest molecule is fully surrounded by host molecules. With the matrix isolation technique, spectra of single molecules in such matrices as rare gases can be recorded.[36,37] Details of the experimental apparatus for the single molecule detection and spectroscopy are described elsewhere.[36-38] Mixture of a rare gas (Xe or Kr) with high-temperature vapours of guest molecules (DBATT or terrylene) is sprayed directly onto the surface of the mirror objective, forming a matrix. The objective is mounted in an electrolytic copper holder and the whole assembly is attached by screws to the cold finger of a cryostat. The matrix deposition procedure begins with pre-cooling the objective down to 40-60 K, then the probe molecules crystals (DBATT or terrylene) are heated inside the nozzle and the rare gas flow starts. When the temperature of the nozzle reaches about 510 K, the objective surface is exposed to the stream (flow rate 1 mmol/h) for about 1 min. The presence of DBATT or terrylene molecules is checked by detection of the fluorescence signal. The deposition procedure is repeated when no fluorescence is observed. After the deposition, the cryostat is filled with liquid helium. The experimental results are shown in Fig. 12. The experiment was performed in a far-field regime and the image shown as a 3-D plot represents the intensity of the fluorescence signal over the observed area for a given fluorescence frequency. The three peaks represent three single molecules. The three 2-D plots in the insets shows the spectra of the three molecules. Molecule γ disappeared half way during the frequency scan, causing a sharp drop in the spectral line shape, indicating perhaps a chemical reaction which quenched the molecule. Such a sudden drop of intensity is very common for single molecules embedded into the matrix with the matrix isolation technique.[37]

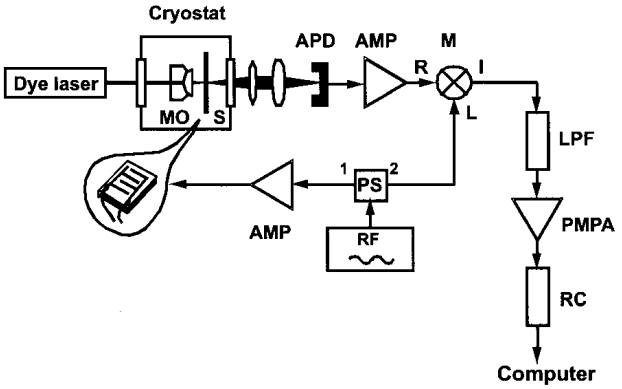

Fig. 20. Schematic plot of the SM absorption experiment setup. MO–microscopic objective, S–sample, APD–avalanche photodiode, RF–RF generator, PS–RF power splitter, AMP–RF amplifiers, M–mixer, LPF–5 MHz low-pass filter, PMPA–postmixer preamplifier, RC–RC circuit.

2.4 Effects, observed on single molecules

2.4.1 Pressure effect

In this section we present the typical results of pressure

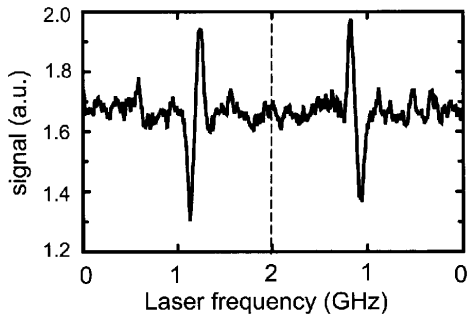

Fig. 21. Single-molecule absorption signal of terrylene in *n*-hexadecane matrix.

effect studies. We begin with the theoretical background of the pressure effect. The transition energy of a single molecule can be presented as:

$$\omega_0 = \omega_0^0 + \delta\omega_0(R) \tag{14}$$

where ω_0^0 is associated with the transition energy between the ground and the first excited states and $\delta\omega_0(R)$ denotes the spectral shift due to the interaction between the guest and host molecules as a function of environment variables. Here R is the distance between the molecule under the study and a solvent molecule. The spectral shift due to a group of host molecules can be expressed as:

$$\delta\omega_0(R) = \frac{K}{R^6} \tag{15}$$

where K is the constant related to the polarizability of the guest molecule. If host molecules are randomly distributed, then we can use

$$\langle\delta\omega_0(R)\rangle = \int_{R_0}^{R_\infty} dR\delta\omega_0(R)\frac{4\pi R^2}{V} = \frac{4\pi K}{3V}\left(\frac{1}{R_0^3} - \frac{1}{R_\infty^3}\right) \tag{16}$$

where $V = 4\pi R_\infty^3/3$, and R_0 represents the nearest distance between the relevant molecule and the surrounding molecule. In the approximation $R_0 << R_\infty$ applies, the spectral shift is:

$$\langle\delta\omega_0(R)\rangle = \frac{4\pi K}{4\pi R_\infty^3}\frac{1}{R_0^6}\left(R_0^3 - \frac{R_0^3}{R_\infty^3}\right) \approx \frac{K}{R_0^6}\frac{V_0}{V}. \tag{17}$$

Using the relation

$$V = V^0\exp(\beta p) \tag{18}$$

where p is the external pressure and β is the compressibility factor, we can see that the spectral shift can be written as

$$\langle\delta\omega_0(R)\rangle = \frac{K}{R_0^6}\exp(-\beta p). \tag{19}$$

This result is obtained under the assumption of a random distribution of host molecules. For a general case, the integration in Eq. (16) should be replaced by a summation.[39]

The experimental setup for studying pressure effect on SM spectra can be found in PhD thesis of Mauro Croci.[9] The cryostat part of the experimental setup is combined with a pressure cell as shown in Fig. 22. The home-built pressure cell consists of a small-volume chamber made of copper, with two quartz windows sealed with indium. The cell fits in the bottom of the cryostat and is connected through a steel capillary to the outside, where a pressure gauge, the helium supply, and the vacuum pump are located. During an experiment the cell is immersed in superfluid liquid helium at a temperature of 1.8 K. Helium condenses in the chamber and in the lower part of the capillary. The pressure of the helium gas in the upper part of the capillary, which is controlled by the gas supply and the vacuum pumps, is transmitted by the condensed helium to the sample. Hydrostatic pressures from 10 to 1000 hPa can be achieved.

The spectra of a single pentacene molecule at 1.8 K at 592.327 nm, measured for different pressure changes relative to the lowest pressure (typically around 15 hPa) and corrected for laser drifts, are shown in Fig. 23. The baseline of the spectra have been shifted vertically, proportional to the pressure change. The projection of the center of the molecule resonance peak onto the baseline is indicated by circles. The molecule resonance shifts with increasing pressure to the red,

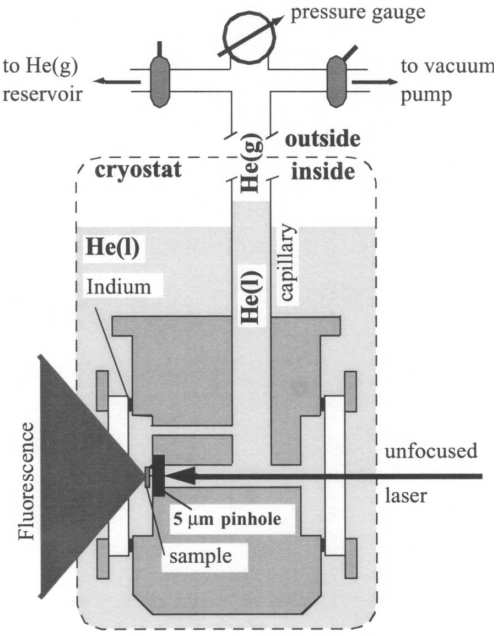

Fig. 22. Pressure Cell. The home-made pressure cell consists of a small volume chamber (~ 1 cm^3) with two windows. The chamber has a capillary, which connects it to a pressure gauge, and two valves, one connected to a helium gas reservoir and the other to a vacuum pump. During operation, the cell is immersed in liquid helium. The capillary reaches out of the cryostat, where the gauge and the two valves are located. Liquid helium condenses in the sample chamber, and acts as a pressure transmitting medium. The pressure changes in the helium gas phase in the upper part of the capillary, which are controlled by the vacuum pump and the helium reservoir, are transmitted to the sample by the liquid.

as emphasized by the solid line. There are no detectable changes in signal strength and width with pressure in contrast to the hole-burning experiments. This observation opens the possibility of extending the experiment to the high pressure regime by following the shift of a single molecule over a greater range, without the drawback of the signal fading. This could be achieved for the molecules which do not undergo spectral diffusion.[40]

The measured shifts Δν of the resonance frequency for 3 different molecules are shown in Fig. 24. Linear fits to the measured data are also plotted. The numbers near the points of molecule M2 (black circles) indicate the temporal sequence in which the data were collected. The shifts were completely reversible within the resolution of our experiments. The slope of the linear fits for the five molecules investigated varied from -0.74 to -1.0 MHz/hPa. The average shift is -0.9 ± 0.1 MHz/hPa.

2.4.2 Stark effect

In SMS literature, Stark effect means the spectral shift of the SM spectral lines with the applied electric fields. The first measurement on single molecules (pentacene in *p*-terphenyl crystal) in an electric field was performed in 1992 by Wild et al.[41] In the following years, Stark effect was measured for different host/guest systems: perylene in *n*-nonane,[14] terrylene in naphthalene,[16] terrylene in polyethylene,[42] dibenzanthanthrene in naphthalene and in *n*-hexadecane,[43] and diperinaphthylenpyren in *n*-hexadecane.[44]

The measured Stark shift of a single molecule's reso-

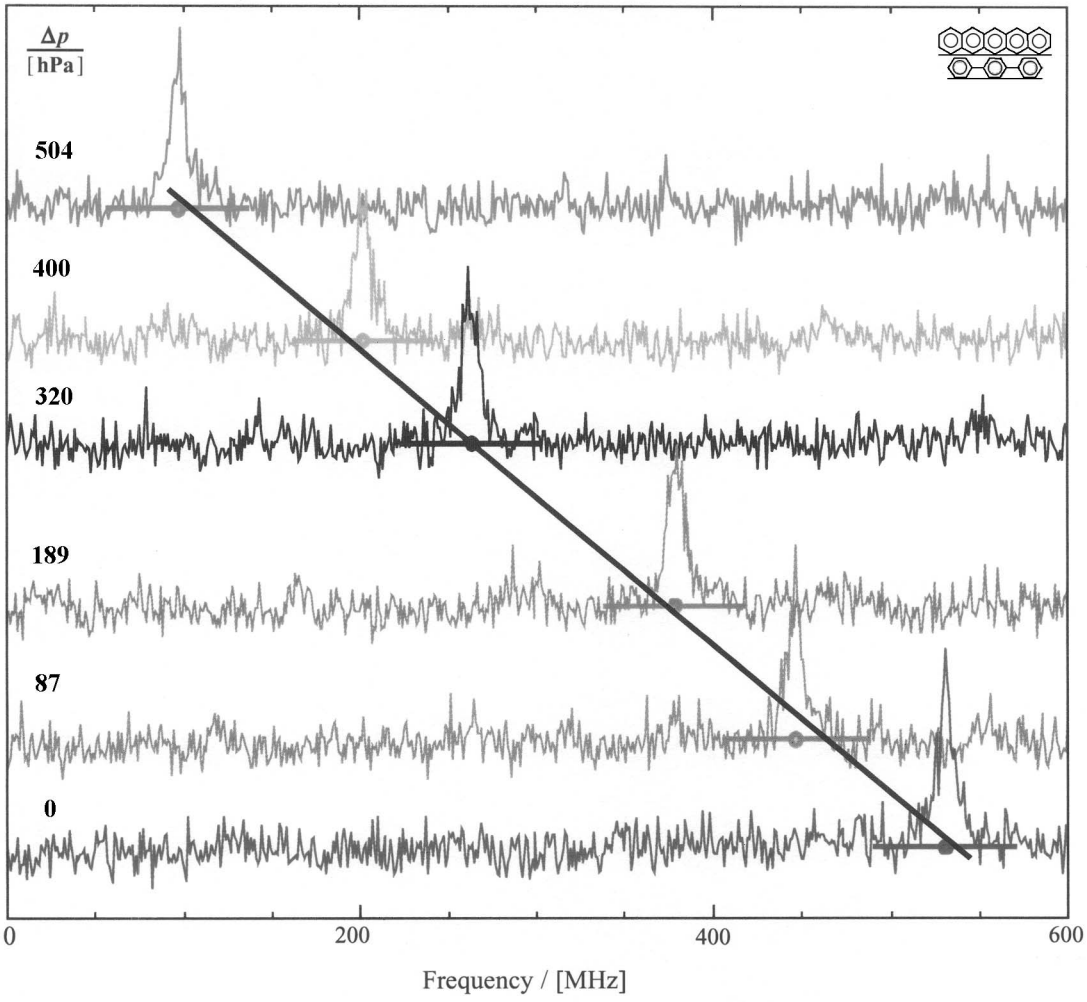

Fig. 23. Fluorescence excitation spectra of a single pentacene molecule at a wavelength of 592.327 nm measured at 1.8 K for different pressures. The pressure differences are relative to the lower spectrum which was measured at 15 hPa. The spectra have been corrected for laser drifts. The solid line indicates a linear shift of the line centers to lower frequencies (emphasized by the gray dots) with increasing pressure.[9]

nance frequency $\Delta\nu$ is:

$$h\Delta\nu = \Delta W(S_1) - \Delta W(S_0) = aE_{ext} + bE_{ext}^2 + \cdots \quad (20)$$

where $\Delta W(S_0)$ and $\Delta W(S_1)$ are the changes of the energy of the molecular ground and first excited states, a and b are the expansion coefficients:

$$a = -\Delta\mu_{ind}\cos\theta f_L, \qquad b = -\frac{1}{2}\Delta\alpha f_L^2 \quad (21)$$

where $\Delta\mu_{ind}\cos\theta$ is the projection of the difference of the induced dipole moments $\Delta\vec{\mu}_{ind} = \vec{\mu}_{ind}^{S_1} - \vec{\mu}_{ind}^{S_0}$ onto the direction of an external electric field, and $\Delta\hat{\alpha}$ is the difference of the polarizabilities in the ground state S_0 and the first excited state S_1: $\Delta\alpha = \alpha_{S_1} - \alpha_{S_0}$. From a measured spectral trajectory of a single absorber in an external electric field, its induced dipole moment (projection) and polarizability can be defined.

When a centrosymmetric molecule is inserted into a polar matrix, its symmetry is broken by strong matrix fields and the molecule gains an induced dipole moment. The more the distortion of the molecule caused by the matrix is, the larger the value of the induced dipole moment is and the larger the linear shift of the molecule's resonant frequency in an electric field is. A recent theoretical work of M. Hayashi et al. is dedicated to the mechanism of the formation induced dipole moment of a guest molecule immersed into a host matrix.[45]

The main part of the experimental setups for performing Stark effect is the electrodes. The electrodes can be a sample sandwich using pieces of ITO glass as shown in Fig. 25;[13] in this configuration E_{ext} is fixed perpendicular to the laser field (see Fig. 26). The electrode system can be also a microchip with interdigitated golden electrodes (see Fig. 27); with this geometry, the polarization of the laser beam and the external applied electric field are co-planar (see Fig. 28).

Linear Stark shifts of several molecules under identical conditions are shown in Fig. 29, where a total laser scan range of 12.1 GHz and an applied electric field strength of -6.7 kV/cm $\leq E_{ext} \leq$ 6.7 kV/cm was performed. The lines plotted in Fig. 29 represent the fluorescence of molecules whose absorption maxima shifted in the (ν_L, E_{ext})-plane. The dark regions are background areas, where no molecules could be excited. From linear Stark trajectory, induced dipole moment of molecule $\Delta\vec{\mu}_{ind}$ can be estimated.

Historically, quadratic Stark effect was the first re-

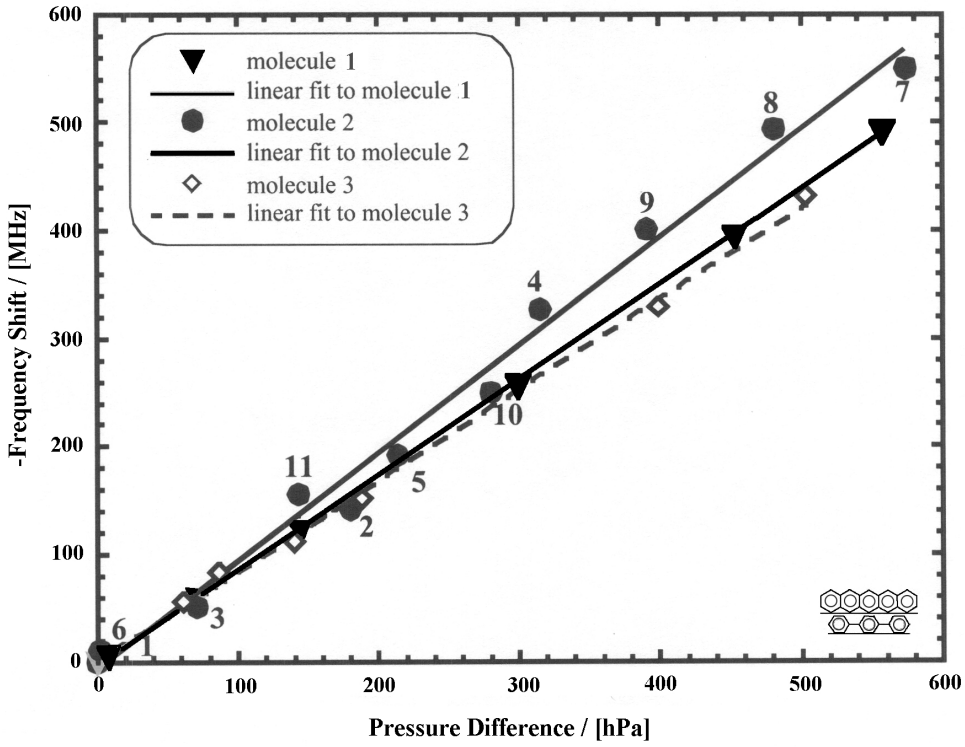

Fig. 24. The spectral shifts of the zero phonon lines are plotted against the changes in the hydrostatic pressure for three different pentacene molecules in the O_1 site of a *p*-terphenyl crystal. Linear fits to the data are also plotted. The numbers indicate the temporal sequence in which the data for molecule M2 (black circles) were collected. The process is completely reversible to within our experimental accuracy.[9]

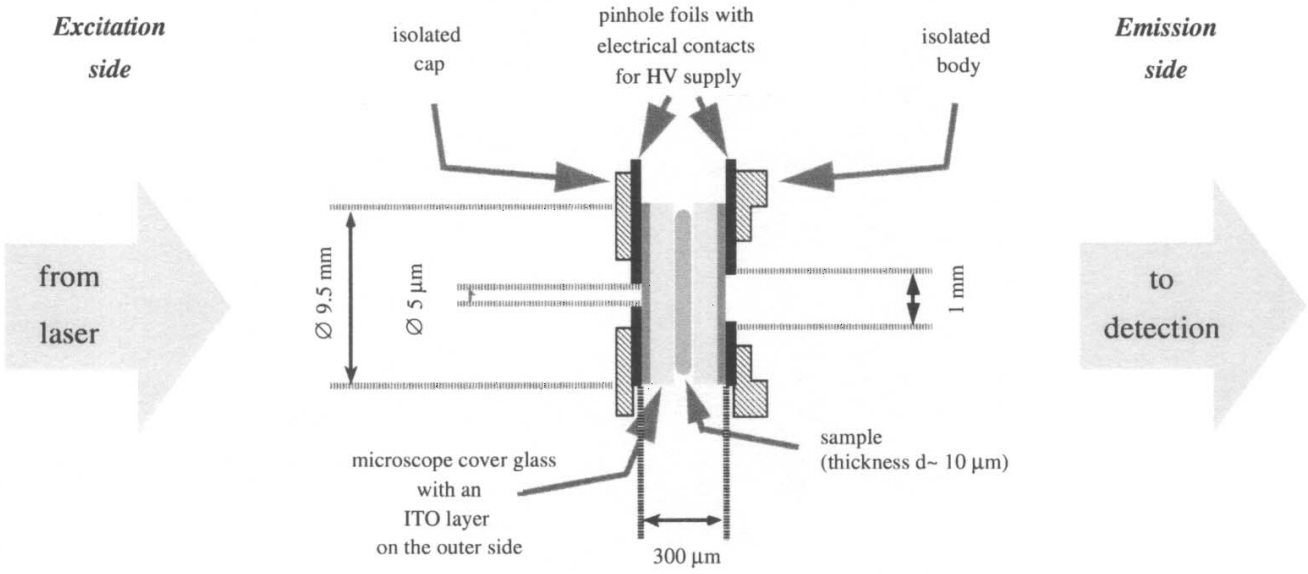

Fig. 25. "Sample sandwich" for Stark effect experiments. Notice that ITO coated cover glasses and an additional pinhole foil is used on the emission side.[13]

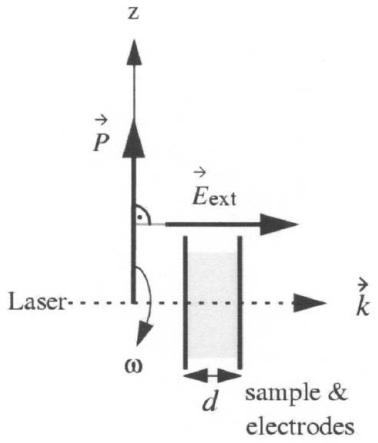

Fig. 26. In the "sample sandwich" configuration of Stark effect experimets, the laser propagation direction $\vec{k}$ is always parallel to $\vec{E}_{ext}$. The polarization $\vec{P}$ is rotated by ω around the *y*-axis to minimize the angle α between $\vec{P}$ and the transition dipole moment of a molecule.[13]

ported Stark effect on single molecules, measured in Wild's group in 1992.[41] Spectra of four single pentacene molecules recorded in that experiment, demonstrating quadratic Stark effect, are shown in Fig. 30. From the quadratic coefficients, the polarizabilities of molecules can be calculated. Report on negative quadratic Stark shifts can be found in the PhD thesis of Hermann Bach.[16]

Recently, a higher-order Stark effect was observed on a dibenzanthanthrene molecule in naphthalene matrix by Christian Brunel and co-workers.[43] Cubic Stark effect was reproduced on several terrylene and diperinaphthylenpyren molecules in hexadecane matrix in Wild's group.[18,44] Two molecules demonstrating higher-order (cubic) Stark effect are shown in Fig. 31. Higher order Stark effect can be explained in terms of inhomogeneous internal field of the matrix.[44]

Different experimental techniques for studying Stark effect in constant and in alternating electric fields can be found in the literature.[14,16,18,44]

2.4.3 Spectral jump

To date, the *spectral jump* phenomena have been one of the most exciting experimental observation in single molecule spectroscopy. An example of spectral jump is shown in Fig. 32. The displayed molecule is spectrally jumping between two states during experiment.

Anderson et al.[46] and Phillips[47] independently introduced a TLS (two-level system) model explaining the "anomalous" behavior of the specific heat and thermal conductivity in glasses. TLSs are the simplest representation of the multidimensional energy surface. At any point within the sample, certain groups of atoms or molecules have access to two (or more) potential energy minima and can switch between these two minima by a tunneling process as, for example, ammonia molecule does. A TLS involves an asymmetric double potential well, (see Fig. 33). The surface consists of three regions

represented by L, R and M. Transitions between the two wells represent changes in the local structure of the material. One or several TLSs distributed randomly in the matrix might interact with a single molecule. At helium temperatures the thermal energy is lower than the potential barrier so that a transition between the wells is caused by tunneling along a generalized coordinate Q_ℓ, which characterizes the degrees of freedom involved. The Q_ℓ coordinate might represent the position of one atom or a center of mass of a larger system, or a rotation angle of some group of atoms. Although the effects of TLSs has been observed in a wide variety of chemically different systems for two decades, the nature of these degrees of freedom is not known. However, to explain spectral dynamics of single molecules at low temperature, the two-level system, is often used.[48-53]

In the system represented by Fig. 33, the Hamiltonian operator is approximately given by

$$\hat{H} = \hat{H}_{\mathrm{L}} + \hat{V}_{\mathrm{M}} + \hat{V}_{\mathrm{R}} = \hat{H}_{\mathrm{R}} + \hat{V}_{\mathrm{M}} + \hat{V}_{\mathrm{L}}. \quad (22)$$

Here $\hat{H}_{\mathrm{L}}$ and $\hat{H}_{\mathrm{R}}$ represent the Hamiltonian operator of L and R, respectively.

For the case in which vibrational relaxation is much faster than reaction, a thermal average should be introduced to write the transition probability W from L to R as[54-56]

$$W = \frac{2\pi}{\hbar} \sum_{\mathrm{L}} \sum_{\mathrm{R}} P_{\mathrm{L}} \left| \left\langle X_{\mathrm{R}} \left| \hat{V}_{\mathrm{MR}} \right| X_{\mathrm{L}} \right\rangle \right|^2 \delta(E_{\mathrm{R}} - E_{\mathrm{L}}) \quad (23)$$

where P_{L} represents the Boltzmann distribution, and X_{R} and X_{L} denote the wavefunctions for R and L, respectively. Sup-

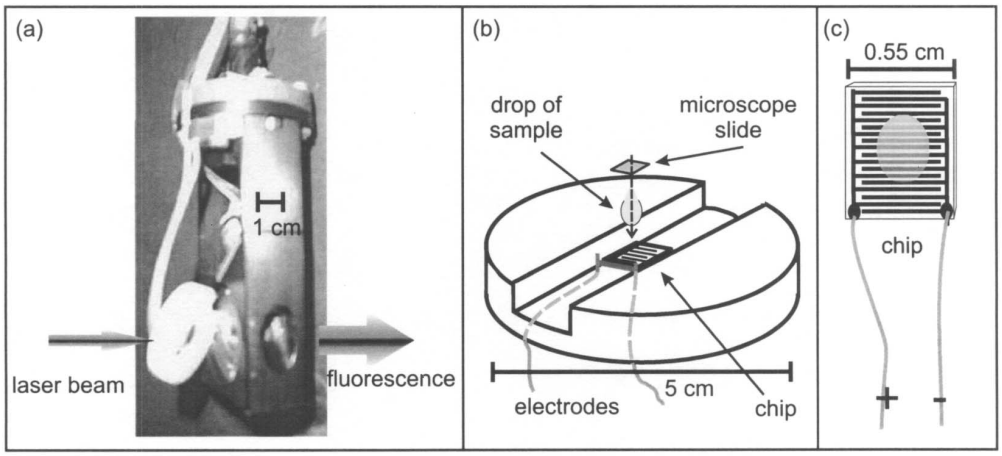

Fig. 27. Sample-holder with electrodes. (a) Picture of the sample-holder. (b) Teflon washer with chip. A drop of sample is placed between the chip and a microscope slide. (c) Pyrex chip with interdigitated electrodes.

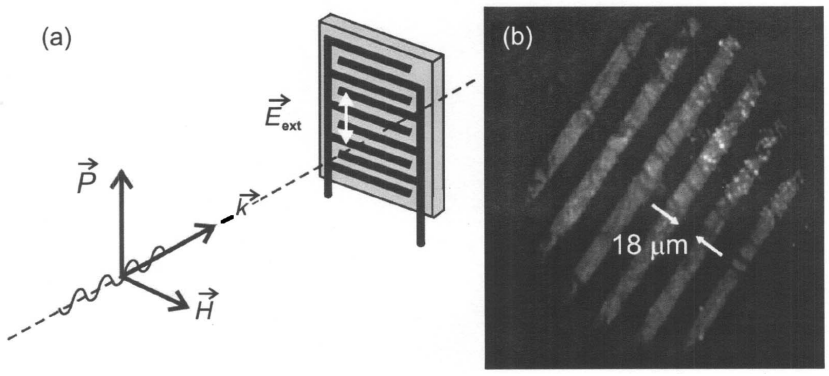

Fig. 28. (a) The geometry of the electric field on the chip with electrodes. $\vec{E}_{ext}$ – externally applied electric field vector, $\vec{k}$ – the laser propagation vector, $\vec{P}$ is the laser polarization vector, and $\vec{H}$ is the magnetic component of the laser beam. (b) Sum of images recorded in white and laser light. The black stripes are the chip electrodes. The bright spots are the fluorescence signals from single molecules. The crystal structure of the sample can be seen.

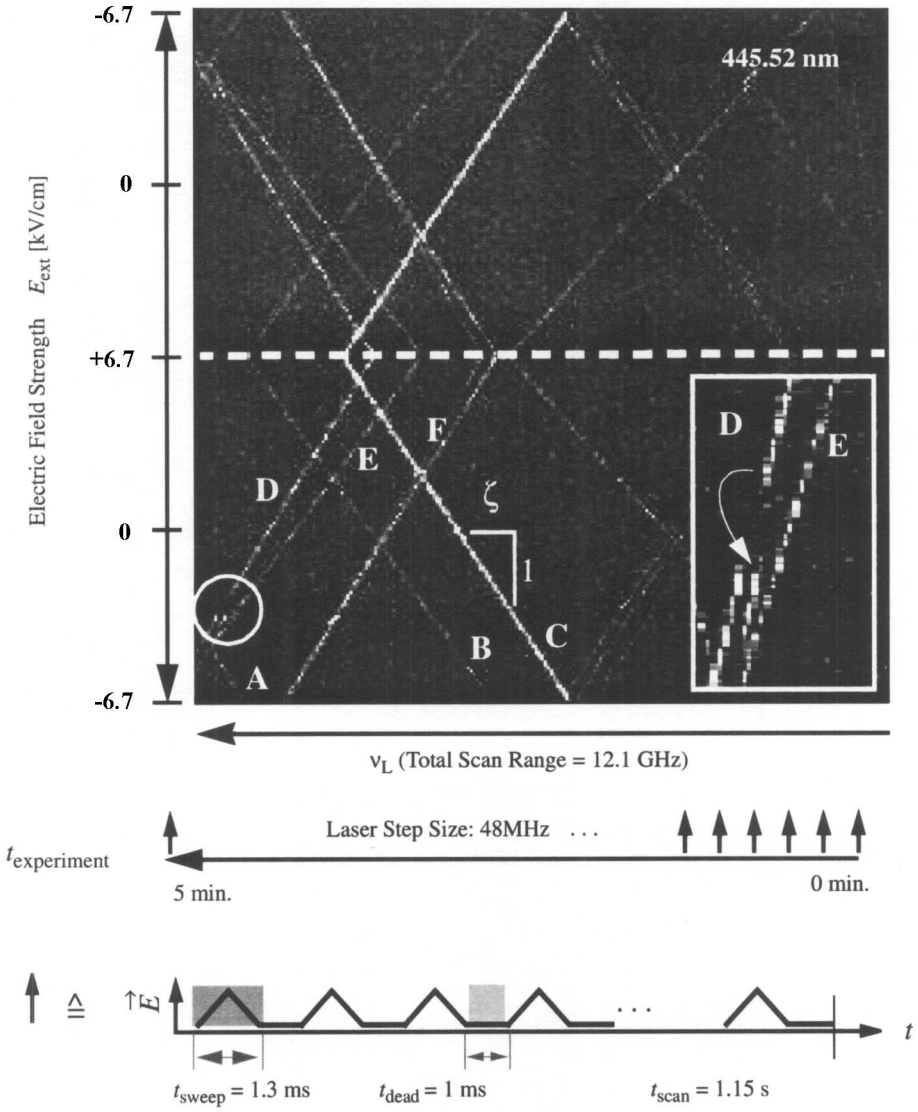

Fig. 29. Molecular linear Stark effect. The most intensely fluorescing molecules are labeled with "A" to "F". The dashed line indicates the mirror symmetry axis in the experiment. The rectangular inset, which is a blown up section of the circled region, shows a spectral jump in Stark trace D. 500 sweeps, accumulated with an electric field ramp repetition rate of 433 Hz, were summed up to obtain one scan at a fixed laser frequency. The laser frequency step size was $\Delta\nu_L$ = 48 MHz.

pose that the transition between L and R is through coupling of one promoting mode ℓ (the reaction coordinate being Q_ℓ), and that we can write the wavefunctions as

$$X_L = \left\{ \prod_i {}' \chi_{Lv_i}(Q_i) \right\} \chi_{Lv_\ell}(Q_\ell), \tag{24}$$

and

$$X_R = \left\{ \prod_i {}' \chi_{Rv_i'}(Q_i') \right\} \chi_{Rv_\ell'}(Q_\ell'), \tag{25}$$

where Q_i is the coordinate of the i-th mode in L and Q_i' is that of the same mode in R, while υ_i and υ_i' are the vibrational quantum numbers of those modes, respectively. χ_{Lv_i} is the wavefunction of the i-th mode in L, and so on. Here we assume that they are harmonic modes. Substituting Eqs. (24) and (25) into Eq. (23) yields

$$W = \frac{2\pi}{\hbar} \int_{-\infty}^{\infty} dt\, e^{it\omega_{RL}^0} G_\ell(t) \prod_i {}' G_i(t) \tag{26}$$

where the time-correlation functions $G_\ell(t)$ and $G_i(t)$ are given

by

$$G_\ell(t) = \sum_{\upsilon_\ell} \sum_{\upsilon_\ell}' P_{\mathrm{Lv}_\ell} \left| \left\langle \chi_{\mathrm{Rv}_\ell'} \mid \hat{V}_{MR} \mid \chi_{\mathrm{Lv}_\ell} \right\rangle \right|^2 e^{it\omega_{\mathrm{Rv}_\ell', \mathrm{Lv}_\ell}} \quad (27)$$

and

$$G_i(t) = \sum_{\upsilon_i} \sum_{\upsilon_i}' P_{\mathrm{Lv}_i} \left| \left\langle \chi_{\mathrm{Rv}_i'} \mid \chi_{\mathrm{Lv}_i} \right\rangle \right|^2 e^{it\omega_{\mathrm{Rv}_i', \mathrm{Lv}_i}}. \quad (28)$$

More complicated cases can be also be treated in the same manner.

For displaced harmonic oscillators, $G_i(t)$ can be expressed as[56,57]

$$G_i(t) = \exp\left[-S_i(2\bar{n}_i + 1) + S_i\{(\bar{n}_i + 1)e^{it\omega_i} + \bar{n}_i e^{-it\omega_i}\} \right], \quad (29)$$

where ω_i is the vibrational frequency of the i-th mode, S_i is the

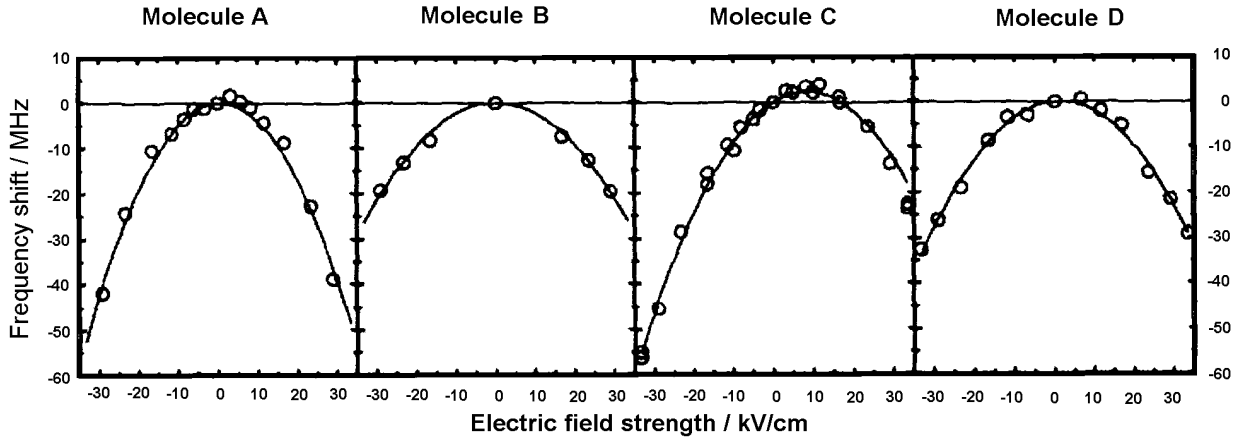

Fig. 30. Quadratic Stark effect measured on four single pentacene molecules in *p*-terphenyl matrix.[41] The circles denote the resonance position of a single molecule.

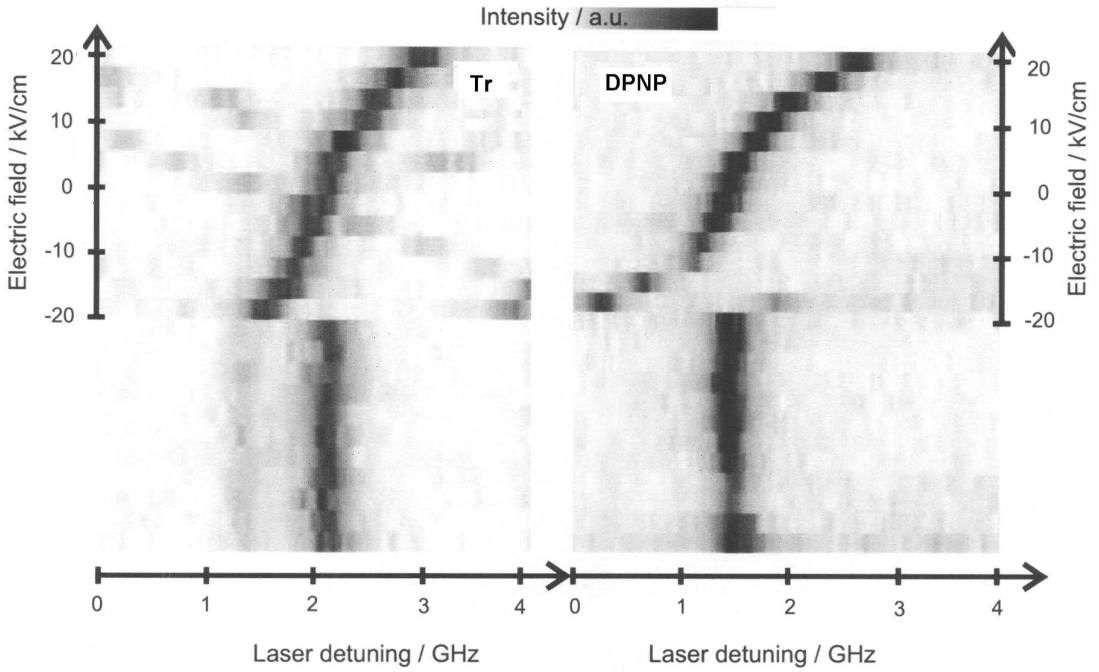

Fig. 31. Two single Tr and DPNP molecules showing a higher order Stark effect. The lower parts of the picture show molecular spectra in the absence of an external electric field. The scans with and without external field were performed in alternating fashion in order to eliminate laser drift from the data.

coupling constant, and $\bar{n}_i$ is the thermal-average occupation number of that mode. That is,

$$S_i = \frac{\omega_i}{2\hbar}(Q_i' - Q_i)^2; \quad \bar{n}_i = 1/\left(e^{\hbar\omega_i/k_B T} - 1\right). \tag{30}$$

Using Eq. (29) we obtain

$$W = \frac{2\pi}{\hbar}\int_{-\infty}^{\infty} dt\ G_\ell(t) \times \exp\left[it\omega_{RL}^0 + \sum_i S_i \left\{ -(2\bar{n}_i + 1) + (\bar{n}_i + 1)e^{it\omega_i} + \bar{n}e^{-it\omega_i} \right\} \right] \tag{31}$$

For the strong coupling case, we can use the short-time ap-

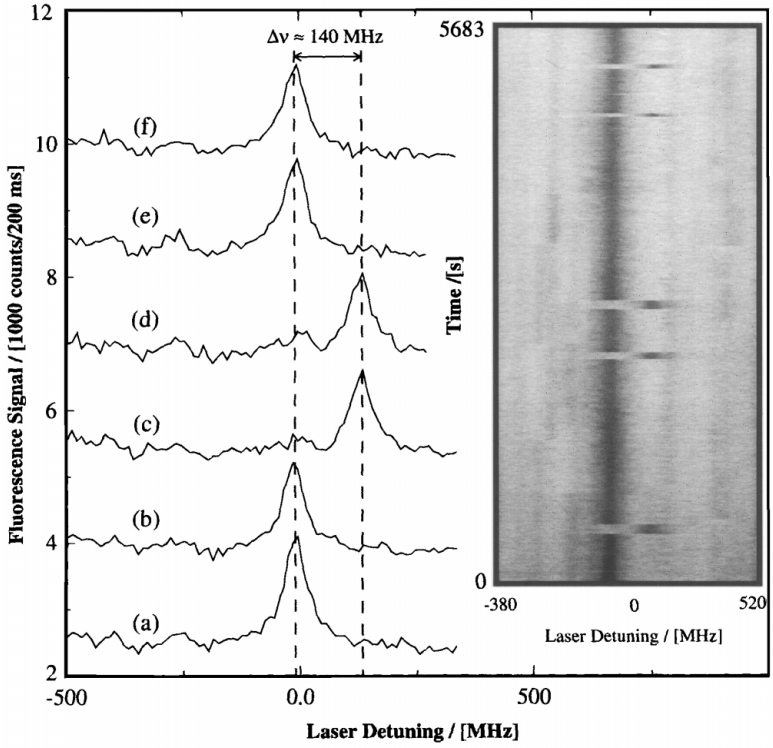

Fig. 32. Resonance frequency changes for a single terrylene molecule. (a)-(f): Six sequential fluorescence excitation spectra with 40 s per scan, 0.32 W/cm^2 laser intensity, and the time between scans varying from 2 to 10 min. Inset: gray-scale image of continuous "fast" 1 GHz (only 90% plotted) excitation spectra. The *x*-axis is the laser frequency detuning, the *y*-axis corresponds to the time axis (scans are plotted consecutively from bottom to top), and the darkness of the image represents the fluorescence intensity. There are a total of 2220 scans acquired over 5683 s, with 10 ms/point, 256 points/scan, and 1.1 W/cm^2 probing intensity.

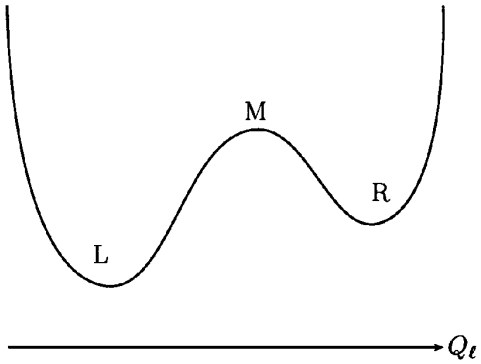

Fig. 33. The two-level model often used in treating the spectral jump phenomena.

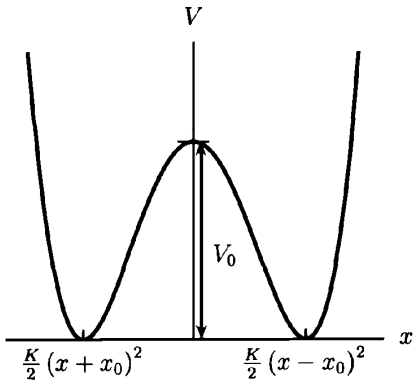

Fig. 34. The particular potential energy surface used in the model of spectral jump in this work.

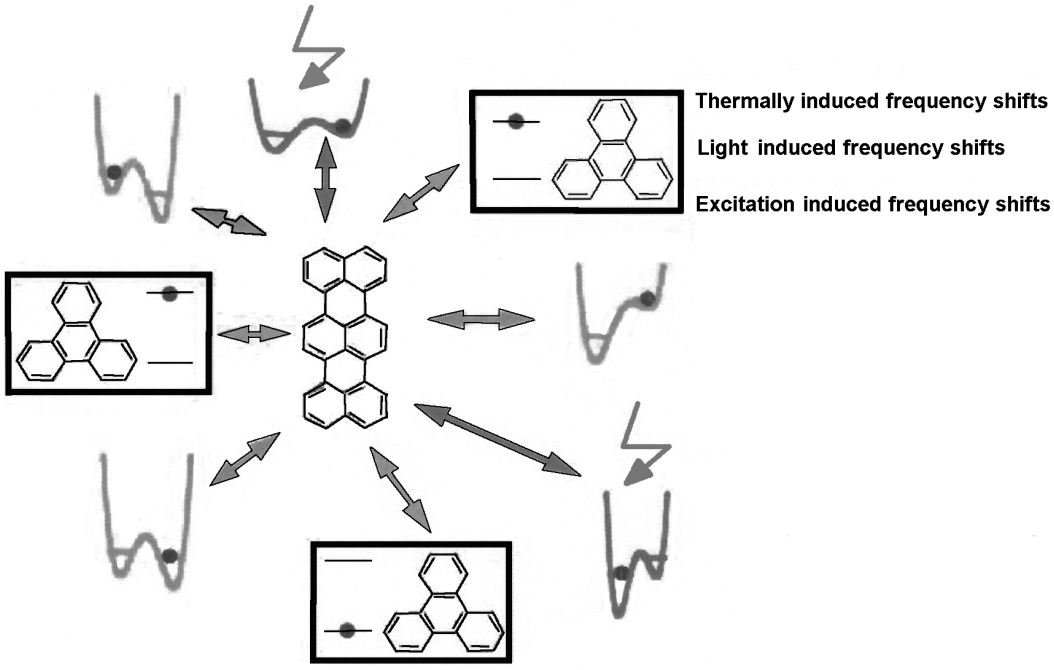

Fig. 35. Frequency shifts of terrylene in hexadecane interpreted by TLS model.

proximation:

$$W = \frac{G_\ell(0)}{\hbar^2}\sqrt{\frac{2\pi}{\sum_i S_i\omega_i^2(2\bar{n}_i+1)}}\exp\left[\frac{-(\omega_{RL}^0+\sum_i S_i\omega_i)^2}{2\sum_i S_i\omega_i^2(2\bar{n}_i+1)}\right] \quad (32)$$

In the classical limit, Eq. (32) becomes Arrhenius equation.

From the above treatment we can see that up to this point, the details of the potential surfaces along the reaction coordinate Q_ℓ is not specified. For this purpose, we consider a particular case,

$$V(x) = \frac{a^2}{4b} - ax^2 + bx^4. \quad (33)$$

Notice that

$$\begin{aligned} V_{MR}(x) &= V(x) - \frac{K}{2}(x+x_0)^2 \\ &= V_0 - \frac{K}{4}x^2 + \frac{K}{64V_0}x^4 - \frac{K}{2}(x+x_0)^2 \end{aligned} \quad (34)$$

where

$$\begin{aligned} &x_0 = \sqrt{\frac{a}{2b}}; \quad V_0 = \frac{a^2}{4b}; \quad K = 4a; \\ &b = \frac{(K/4)^2}{4V_0}; \quad x_0 = \sqrt{\frac{8V_0}{K}}. \end{aligned} \quad (35)$$

For the approximate case $G_\ell = |\langle\chi_{R0_\ell'}|V_{MR}|\chi_{L0_\ell}\rangle|^2$, we find

$$G_\ell = \left[V_0 e^{-8/\varepsilon}\left(-3 - \frac{3\varepsilon}{8} + \frac{3\varepsilon^2}{256}\right)\right]^2 \quad (36)$$

where

$$\varepsilon = \frac{K_\ell}{V_0}\frac{\hbar}{m\omega_\ell} = \frac{K_\ell}{V_0}\frac{\hbar}{\sqrt{mK_\ell}} = \frac{\hbar}{V_0}\sqrt{\frac{K_\ell}{m}} = \frac{\hbar\omega_\ell}{V_0}. \quad (37)$$

If $\varepsilon << 1$, then

$$G_\ell = (-3V_0 e^{-8/\varepsilon})^2 = 9V_0^2\exp\left(-\frac{16V_0}{\hbar}\sqrt{\frac{m}{K}}\right). \quad (38)$$

That is, G_ℓ shows an isotope effect. For example. for hydrogen H and deuterion D, we have

$$G_\ell(D) < G_\ell(H). \quad (39)$$

In other words, the transition is slower for heavier isotopes. Thus a correct tendency is predicted.

Asymmetric double well model can also be solved in the similar manner, and it is more suitable for describing the spectral jump phenomena in SM, but the algebra involved is more complicated so we do not discuss it further here.

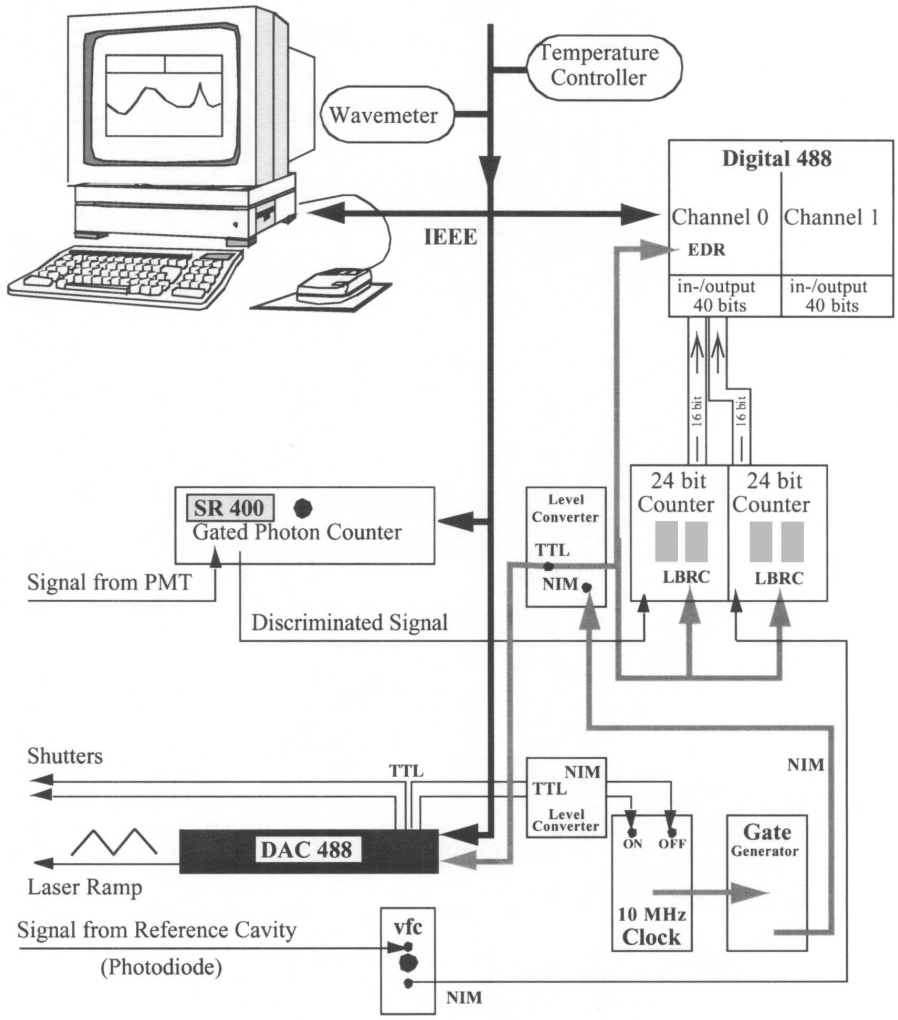

Fig. 36. Detection electronics. An external clock (and a time divider) gives the timing (dashed line) to the experiment. Upon receiving a trigger signal in their LBRC-inputs, the binary counters load their buffers with the current data and reset the counter. The data are read from their buffers by Digital 488, which receives the same trigger pulse in its EDR-input. The signal consists of 40 bits divided in two times 16 bits from the counters and 8 bits not used. This data is then transferred to the computer. The laser frequency is driven by a digital-to-analog converter. A voltage ramp is stored in its buffer, and upon receiving a trigger signal, the device is programmed to output the next value stored in its buffer.[9]

3. SINGLE MOLECULES AT ROOM TEMPERATURE

A big advantage of doing room temperature single molecule detection is an opportunity to perform biological experiments. A scheme of confocal setup for detection single molecules at room temperature is shown in Fig. 38. In this configuration, the illumination spot size is diffraction limited and is in order of nm. Figure 39 shows a wide-field illumination setup which can be obtained from confocal setup by introducing a lens into the excitation beam, which enlarges the laser spot up to 10-20 μm in diameter. Thus, a room temperature experimental setup can be switched between confocal and wide-field illumination by inserting a flipping lens. The molecules are excited at an average power of 500 W/cm.[2]

3.1 "Oxygen" effect

One of the easiest and most demonstrative room temperature single molecule experiment is the observation of triplet lifetime quenching by molecular oxygen.[58] Images taken during such an "oxygen" effect experiment are shown

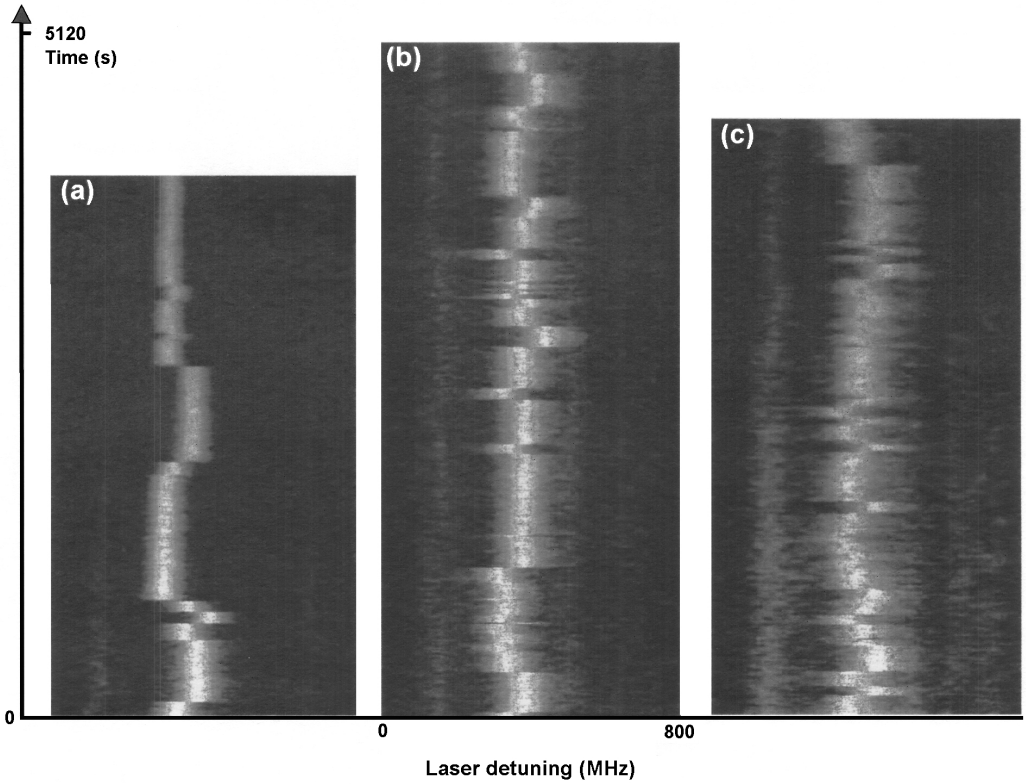

Fig. 37. Three scans over the same terrylene molecule, excited with three different laser powers. Spectrum(a) was recorded with 350 mW/cm^2, and consists of 1540 scans lasting ≈ 58 min. Spectrum (b) was recorded with 1 W/cm^2, and consists of 2000 scans, ≈ 85 min long. Finally spectrum (c) was recorded with 3.1 W/cm^2, and consists of 1680 scans, ≈ 71 min long.[9]

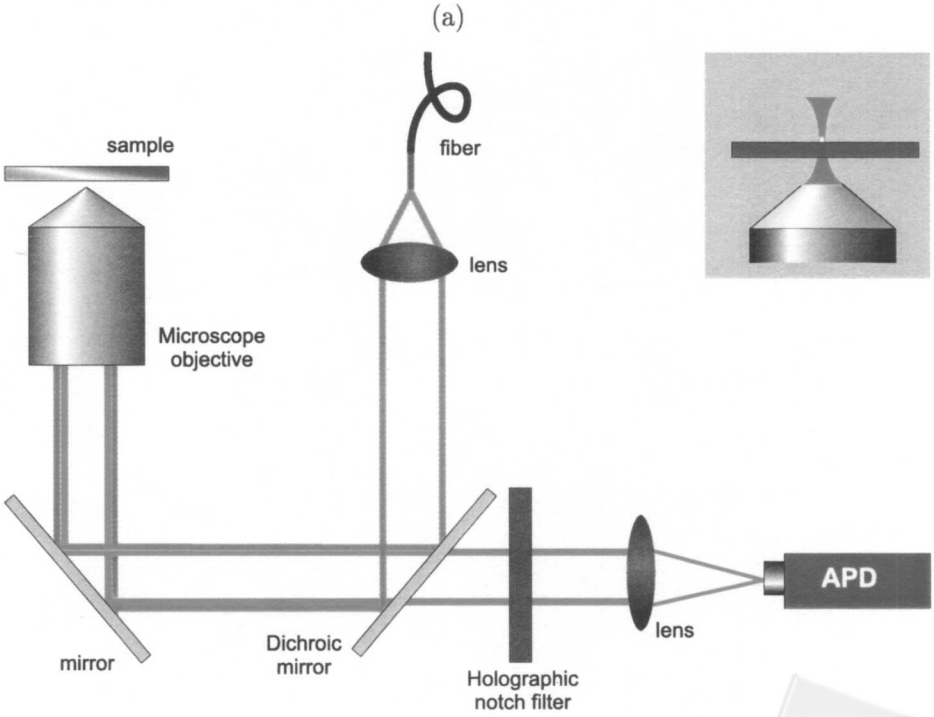

Fig. 38. Confocal setup for room temperature single molecule microscopy.

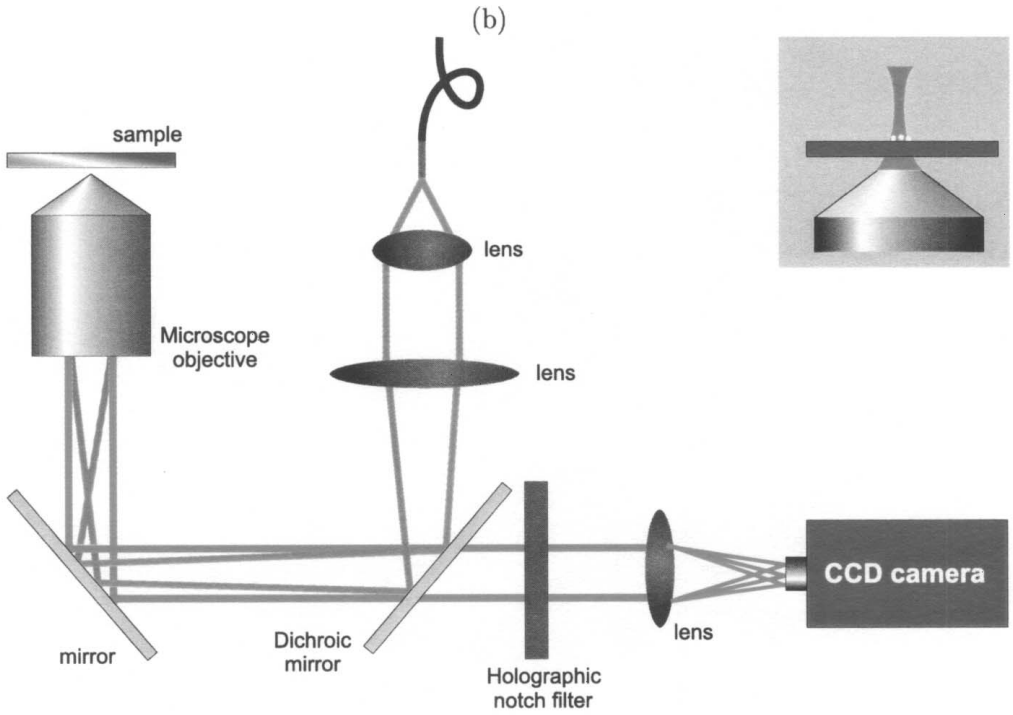

Fig. 39. Confocal setup switched into regime of wide-field illumination.

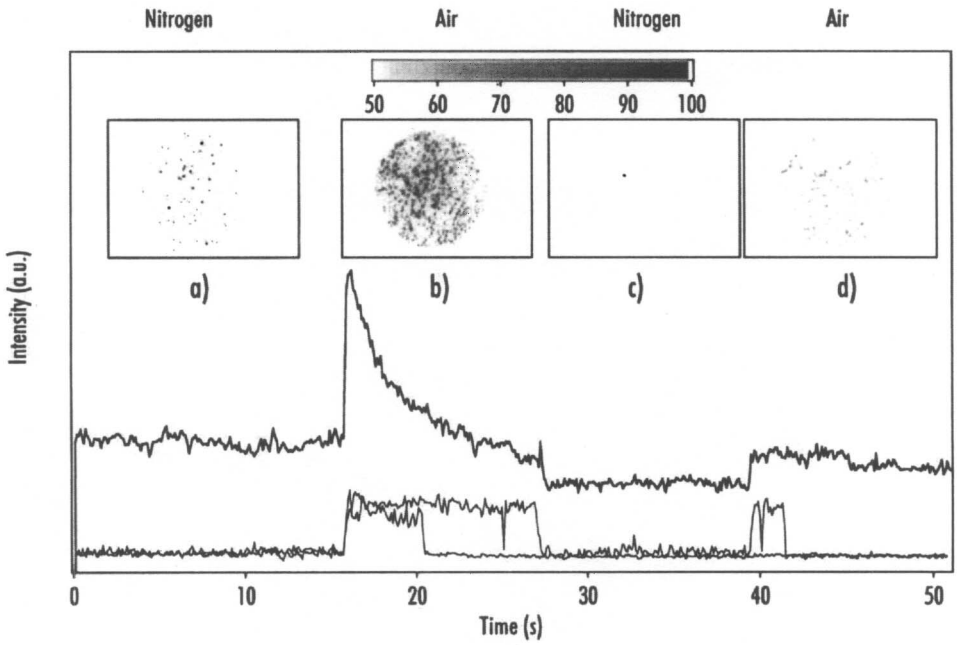

Fig. 40. Sequence of images illustrating the influence of oxygen on the fluorescence intensity of individual DiI_{18} molecules when the sample is flushed with nitrogen [(a) and (c)] and oxygen [(b) and (d)], respectively. Below the integrated intensity of a sequence of 510 images is plotted. The intensity time traces of two individual spots illustrate the photochemical bleaching[58]

in Fig. 40. The probe molecule was DiI_{18} embedded into a PMMA matrix by the spin-coating technique. The sample was flashed with oxygen and nitrogen, while images were acquired with a CCD camera (wide-field configuration of the setup). The recorded images clearly show increase of the intensity when the sample was exposed to air (oxygen), and almost complete "off" intensity when the sample was exposed to nitrogen flow. In Fig. 40, images taken at an integration time of 100 ms impressively illustrate the effect of oxygen when the nitrogen flow to the sample is stopped and switched on, respectively. The number of fluorescing single molecules decreases during exposure to air due to photochemical bleaching.

By positioning individual molecules within the confocal volume of the SCOM system (actually the experimental setup is "switched" into the SCOM configuration as described above), the transient intensity shown in Fig. 41 was obtained by counting single-photon detection from a single molecule. The distribution of the "on" and "off" time of the fluorescence has been analyzed over 248 DiI_{18} molecules.[58] It is found that, during exposure to oxygen, the triplet lifetime was lowered by two orders of magnitude. The quenching effect was shown to dramatically increase the average emission intensity in comparison to the absence of oxygen. With further analysis, it was found that the (radiative) decay time from S_1 to S_0 was 3.3 ns, and the triplet lifetime of T_1 was about 320 μs. The intersystem-crossing quantum yield Y_{ISC} was determined to be 3.3×10^{-4} (see the summarizing diagram in Fig. 42).

3.2 Rotary motion of F_0F_1 ATP synthase

This subsection is dedicated to the single molecule room temperature observation of ATP. ATP is the universal biological energy source; it is formed by F_0F_1 ATP synthases from ADP and inorganic phosphate with the use of energy from a transmembrane ion potential established by photosynthetic or respiratory processes. F-type ATP synthases are widely distributed in nature and occur in the cytoplasmic membrane of bacteria, the inner membrane of mitochondria and the thylakoid membrane of chloroplasts. All known F_0F_1 ATP synthases show conserved structural and functional features and are composed of two distinct subcomplexes termed F_1 and F_0. The F_1 sector is membrane-associated and harbors the catalytic sites of ATP synthesis, while the F_0 sector is membrane-intrinsic and contains the coupling ion translocation machinery. The elucidation of the structure and the enzymatic mechanism of F_0F_1 earned Paul D. Boyer and John E. Walker the 1997 Nobel Prize for Chemistry.

In the case of *P. modestum*, ATP synthase comprises eight different subunits with a stoichiometry of $\alpha_3\beta_3\gamma\delta_\varepsilon$ for F_1

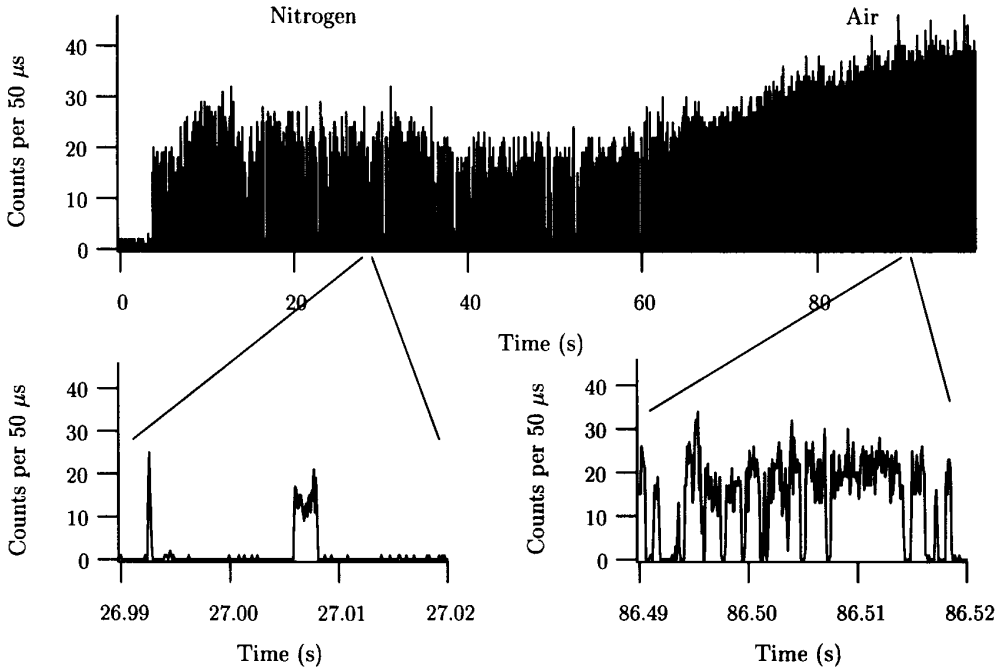

Fig. 41. Fluorescence intensity time trace of a single molecule under being flushed with nitrogen and air (oxygen). The arrow indicates the termination of the nitrogen flush. It can be seen from the two lower pictures that, while the intensity of the emitted fluorescence remains constant, the duration of the dark periods is changed.[58]

and ab_2c_{11} for F_0 (see Fig. 43). As indicated by electron micrographs, the F_1 moiety is connected to the F_0 sector via a peripheral stalk, formed by subunit δ and the subunit *b* dimer, and a central stalk, formed by the ε and γ subunits.[59] An electron density map obtained from crystals of a yeast subcomplex comprising all F_1 and the *c* subunits of F_0 showed a ringlike arrangement of 10 *c* subunits which are in close contact with the central stalk units γ and ε.[60] The X-ray structure of the $\alpha_3\beta_3\gamma$ portion of bovine F_1 revealed an alternating hexagonal arrangement of three α and three β subunits around a centrally located γ subunit, which interacts asymmetrically with the catalytic β subunits.[61] This finding led to the proposal of a rotational catalysis, triggered by the γ subunit (Binding Change Mechanism[62]).

To drive ATP synthesis, ions flow along an electrochemical gradient through the F_0 part down the interface between the *a* subunit and the c_{11} complex. The unique structure of this interface permits the F_0 motor to convert the transmembrane ion motive force into a rotary torque. The key feature of the *c* subunit is that the ion-binding site, consisting of

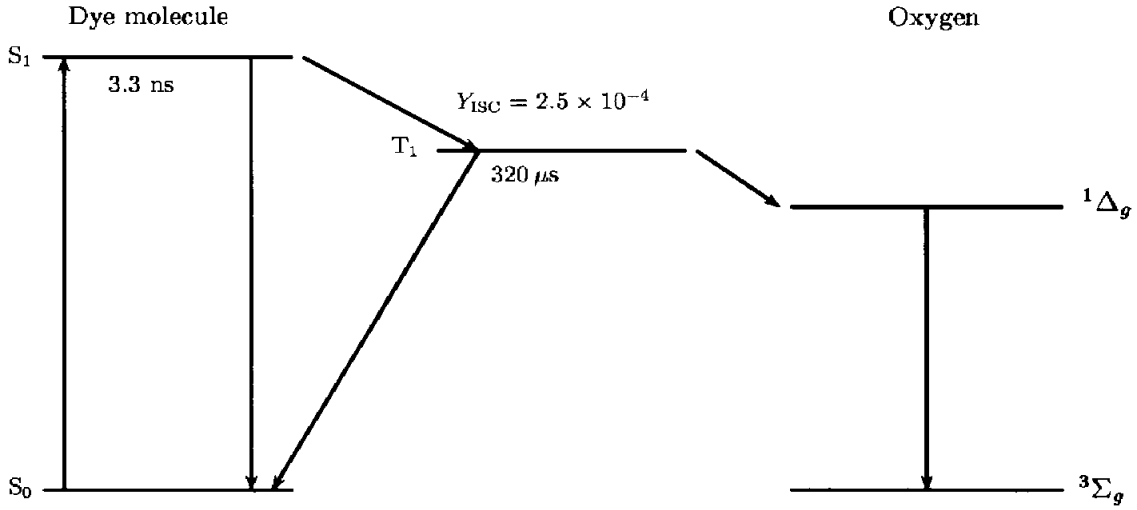

Fig. 42. The rates of the dynamic processes related to the fluorescence property of DiI_{18} molecule observed in the "oxygen" experiment. Y_{ISC} stands for the inter-system crossing quantum yield from S_1 to T_1.[58]

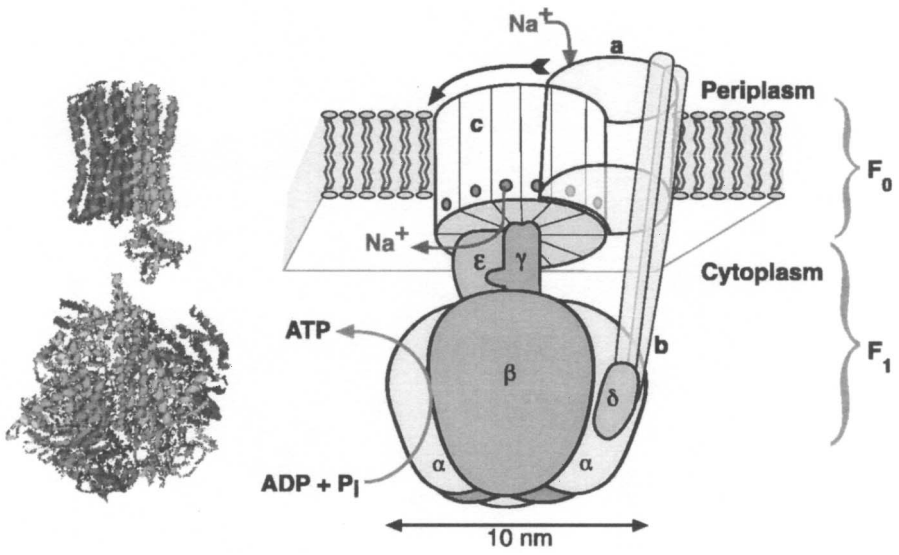

Fig. 43. Left: X-ray structure of the mitochondrial F-ATPase from *S. cerevisiae* at 3.9 Å resolution [102]. Right: Drawing describing the sub-unit composition of the Na^+-translocating F-ATPase from *P. modestum*.[63]

Q32, E65 and S66 (Fig. 44 left), is probably located at the cytoplasmic side of the membrane. Thus the sodium ion binding sites of the rotor have direct access to the cytoplasm. To describe the consecutive stages of ion transport, the illustration in Fig. 44 has been taken from Ref. 63. Rotational diffusion eventually carries an unoccupied, negatively charged site into the hydrophilic strip at the right edge of the stator (A). Once inside, it is quickly captured by the Coulomb attraction of the stator charge, Arginine R227 (B). By thermal fluctuations the site can escape in both directions. Since the entrance channel is aqueous, most of the membrane potential drops across the hydrophilic strip. Therefore, it is more likely for the site to move to the left than to the right. This way, the vertical potential gradient is converted to a driving force acting tangentially to the rotor. A rotor site that fluctuates to the left cannot pass through the dielectric barrier that forms the left side of the channel, for this requires more than 45 k_BT (C). However, once exposed to the periplasmic channel it will quickly pick up an ion, thus neutralizing its charge (D). It is now free to cross the barrier (E), lose the ion into the cytoplasm, and then it cannot diffuse backwards into the stator (F). The motion to the left is additionally aided by the capture of the next free binding site, reflected by the maximum in the dashed line. One cycle decreases the free energy of the system by an amount equal to the electromotive force: $\Delta\mu = \Delta\psi - 2.3(RT/F)\Delta pNa$, where R is the Rhydberg constant, F is the Faraday constant, and pNa is the negative logarithm of the Na concentration. To produce ATP at the observed rate of 30-50 s^{-1} the rotor must exert a torque of 40-50 pN·nm.

This torque is transferred from the F_0 to the F_1 part by the coiled-coil structured γ subunit. The rotation of the γ subunit in turn induces conformational changes in the catalytic sites of ATP sythesis at the β subunits. Finally these conformational changes trigger binding, phosphorylation, and release of the nucleotides.[64] ATP synthesis is strictly dependent on the membrane potential, but is accelerated in the presence of sodium ions.[65] The motor action is completely reversible. During ATP synthesis the motor turns clockwise if viewed from the periplasmic side of the membrane. However, if no membrane potential is applied and ATP is present, the enzyme hydrolyses ATP and turns counter-clockwise.[66]

A number of single-molecule experiments have been performed in the hydrolysis mode using only the F_1 part. Video microscopy was used to monitor the rotation of a micron-sized dye-labeled actin filament attached to subunits γ[66] or ε,[67] respectively, or the rotation of a gold bead attached to the γ subunit.[68] Single-fluorophore polarization microscopy further provided prove that the drag of the filament has only a minor effect on the enzyme's activity.[69] These results offered valuable information on the dynamics of the F_1 motor. The rotation occurs step-wise in three double steps. Each previously reported 120° step[70] is actually composed of one 90° step upon ATP binding ([ATP] dependent), and one 30° step upon ADP release (about 2 ms later).[68] The torque of about 40 pN·nm during rotation remains constant over a broad range of speed, load, and ATP concentration.[71] The energy conversion efficiency approaches 100%: Nearly all of the energy provided by ATP hydrolysis (ΔG = -100 pN·nm) is converted into mechanical work.

Several single-molecule studies went towards observing the rotation of the intact F_0F_1 holoenzyme during ATP hydrolysis. However, the first claim for observing a rotating *c*

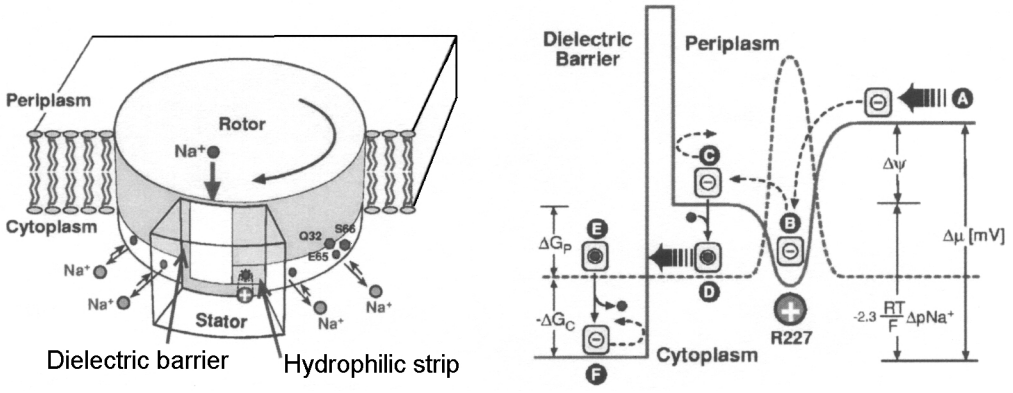

Fig. 44. Model proposed by Dimroth[63] describing the rotor activity of F_0 in terms of potential profiles and thermal ratchets. Left: sketched structure of the ion channel. The sodium binding site is formed by residues Q32, E65 and S66. Right: Free energy diagram for an ion binding site in the vicinity of the channel. The solid line is the potential seen by an unoccupied, negatively charged binding site; the dashed line is seen by an occupied, neutral site. For more detailed explanations see text.

subunit[72] was doubtful, because rotation could only be observed in the presence of detergent and could not be blocked by F_0 specific inhibitors. A probable explanation is that the F_0 sector of the complex had lost its structural integrity.[73] In biochemical studies evidences for a co-rotation of subunits *c* and ε have been obtained indirectly by chemical cross-linking.[74] Each of these studies suffers from the fact that the coupling between rotation during ATP hydrolysis and ion transport, typical for F_0F_1 complexes under physiological conditions, was severly disturbed and could never be observed in single-molecule approaches applied so far.[75] Thus, a challenging question was whether the functionally active F_0F_1 holoenzyme shows a coupled rotational behaviour during ATP hydrolysis and, more fundamentally, whether rotation can be observed in the ATP synthesis mode of the enzyme.

To address these two questions the polarization-resolved confocal microscopy has been used, and the rotation of an individual fluorophore, specifically attached to the *c* subunit of the whole F_0F_1 ATP synthase, was monitored. Coupling of ion transport during ATP hydrolysis is studied on holoenzymes directly immobilized on a cover slip. To observe rotation during ATP synthesis, the enzyme was incorporated in liposomes for application of a membrane potential.

Fluorescence-polarization-resolved confocal microscope was the major tool employed for these studies. The detail of such experimental techniques and the studies performed on F_0F_1 ATP synthase has been described in a thesis[76] and several articles.[77,78]

The sample system that was studied was a hybrid protein consisting of the F_0-part and the δ subunit of *Propionigenium modestum*, a chimeric *P. modestum*/*E.coli* α subunit, and the βγε-part of *Escherichia coli* (G. Kaim, unpublished results). The *a*, *b*, and *c* subunit and the F_1-part of the enzyme were overexpressed separately in *E. coli* and were subsequently purified. In order to reconstitute the holoenzyme, the lipophilic F_0-part was reconsituted into liposomes and the hydrophilic F_1-part was added. After the reconsituted liposomes were incubated with 1% detergent (Triton X-100) the protein was purified by affinity chromatography and stored in liquid nitrogen.

The cyanine dye Cy3 was chosen as a label and the experimental procedure of Adachi et al.[69] was followed. Only the *c* subunits are labeled by cysteine maleimide chemistry. Then, the proteins are immobilized on a glass surface. The immobilization chemistry is based on the well documented histidine nickel chelate complex. This procedure leads to protein immobilization with sufficiently low mobility to observe rotation of the F_0 subunit.

The polarization-resolved fluorescence emission intensity of single proteins described above is detected. A schematic representation of the sample and its environment under which the experiment was performed is shown in Fig. 45. The exciting laser light is circularly polarized. Rotation of the fluorophore is observed by computing the emission polariza-

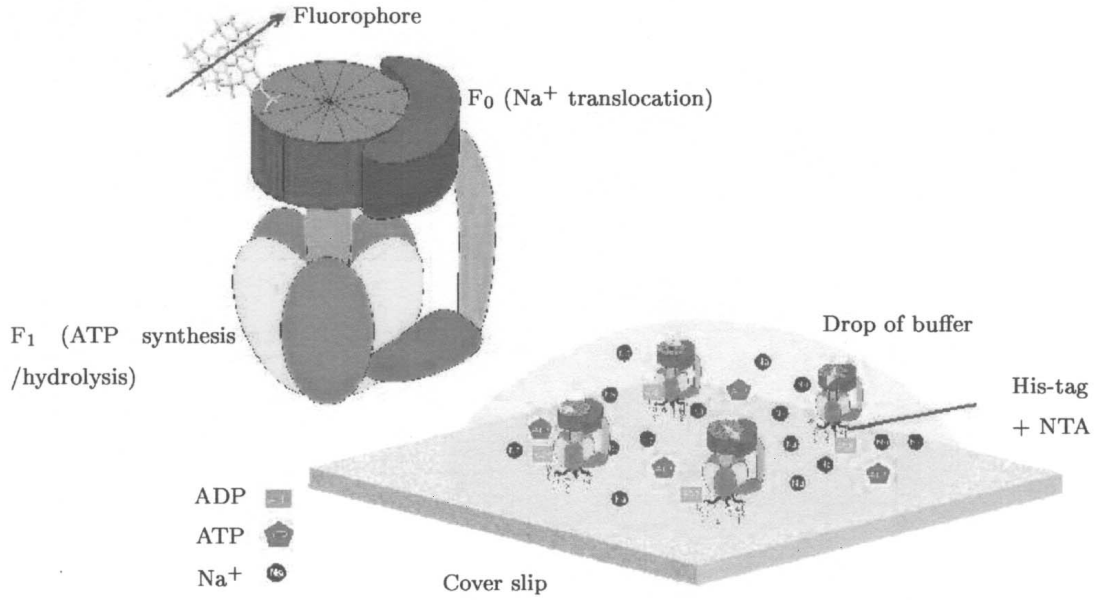

Fig. 45. Schematic representation of the preparation of sample for experimental observation of the rotation of ATP synthase under different concentration of ATP or Na^+.[76]

tion

$$P = \frac{I_{\parallel} - I_{\perp}}{I_{\parallel} + I_{\perp}} \tag{40}$$

which does not depend on the emission intensity. Since the emission dipole has no intrinsic direction, rotation of the dipole by 180° leads to a modulation of the polarization by an entire period.

The time resolution of single-molecule experiments is limited by shot noise of the fluorescence intensity. Under the described conditions, individual steps can not be resolved at high ATP concentrations. By exploiting autocorrelation techniques it is possible to increase the time resolution by averaging over a certain time interval. The autocorrelation function ACF used here is defined as

$$\mathrm{ACF}(t) = \frac{\left\langle [P(t'+t) - \bar{P}][P(t') - \bar{P}] \right\rangle}{\left\langle [P(t') - \bar{P}]^2 \right\rangle}. \tag{41}$$

Some of the properties of the ACF are:[79,80] (1) For a periodic signal, the ACF is also periodic with the same frequency. (2) On the other hand, a random process, like stepping with exponentially distributed dwell times leads to an exponentially decaying ACF, which has additional periodic contributions. (3) The ACF of white noise is 1 at time-lag 0, and 0 otherwise. (4) The Fourier transform of the ACF of a time-series is equal to its power spectrum.

Figure 46 shows examples of the polarization signal of single F_0F_1 ATPases, immobilized via His-tags at the β subunits. The first two traces were recorded in sodium-free buffer containing 0.5 μM ATP (Fig. 46 (a) and (b)). The polarization of +0.65 and -0.5 indicate a constant steady state orientation and low rotational mobility of the fluorophore as well as the whole protein. In most of the observed molecules, well oriented fluorophores were found. Interestingly, in the presence of ATP only (0.5 μM), no rotation was observed. However, after addition of 2 mM sodium chloride (saturation conditions) discrete orientational steps could be resolved (Fig. 46 (c) and (d)), similar to previous experiments.[67,69,70] The fact that Na^+ ions are obligatory for rotation reflects the tight chemo-mechanical coupling typical for F_0F_1 holoenzymes under physiological conditions.

At higher ATP concentration these steps could not be resolved any more due to the insufficient signal to noise ratio. Also see Adachi et al.[69] The use of auto-correlation techniques enabled us to analyze rotation even at saturating ATP and sodium concentrations. First, the polarization time-series

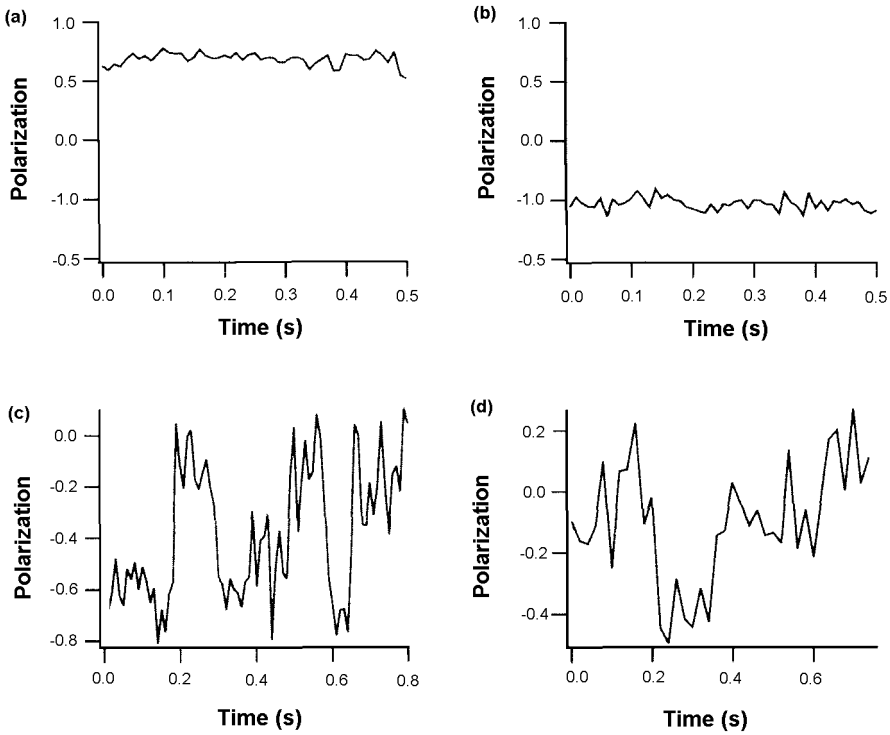

Fig. 46. Typical time-series of the polarization of immobilized F_0F_1 ATPases without [(a) and (b)] and with 2 mM sodium [(c) and (d)]. The ATP concentration was in both cases 0.5 μM. Discrete steps are clearly visible only in the presence of Na^+ ions.[76]

(Fig. 47(a)) and the corresponding auto-correlation function (ACF) of a slowly stepping enzyme at 0.5 μM ATP is shown (Fig. 47(b)). The time series has a periodicity of about 150 ms, leading to an ATP hydrolysis rate of 10 s^{-1}. The stepping rotation is reflected in the ACF by the slow decay at short times. The distance to the first maximum is again about 150 ms. At ATP saturation conditions fast rotation leads to a fluctuating polarization signal (Fig. 47(c)). Fig. 47(d) shows the corresponding ACF with a fast decay and pronounced oscillations of about 20 ms periodicity. The inset shows magnified ACFs of three individual enzymes with similar kinetics. The decay and the first minimum are reproducible, whereas subsequent oscillations are different from molecule to molecule. Without sodium the decay and the oscillations in the ACF are absent, even at high ATP concentration.

The yield of rotating single molecules can be deduced by counting the number of rotating and non-rotating ATP synthases. It is found that 90% of all observed ATPases show no rotation in sodium-free buffer with or without ATP. From the selected molecules, about 80% rotate after addition of Na^+. This is the highest yield of functional F-ATPases reported so far. It has to be compared to about 0.4%[72] and 5%[75] in other studies.

Using the reconstituted F_0F_1 holoenzyme, consisting of the sodium translocating part (F_0) and the ATP synthezising part (F_1), the rotary motor can be also run in the ATP synthesis mode. In order to do so, F_0F_1 was incorporated in monodisperse liposomes (≈ 100 nm diameter).

To start the ATP synthase activity, a sodium motive force had to be generated. At this point a sodium gradient equivalent to 60 mV but no membrane potential is present. Under these conditions no rotation can be observed (Fig. 48(a)). Addition of valinomycin, a hydrophobic ionophor for potassium, increases the membrane's permeability for potassium dramatically. In this way, a potassium/valinomycin diffusion potential was established leading to an influx of potassium ions. As demonstrated previously, it is the voltage component of the electro-chemical Na^+ gradient that finally initiates ATP synthesis.[65] Under these conditions rotation of F_0F_1 during ATP synthesis can be observed (Fig. 48(b)). A change in directionality of the rotation compared to ATP hydrolysis can not be resolved with single-fluorophore experiments.

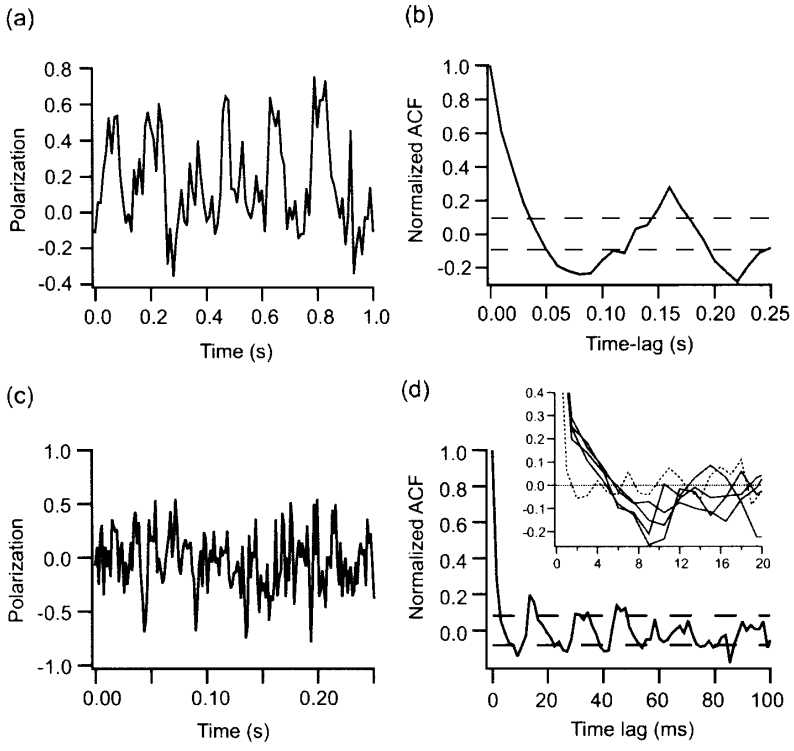

Fig. 47. Time-series of the polarization again with 0.5 μM ATP and 2 mM Na^+, showing discrete steps (a), and with 50 mM ATP, where the stepping rate is too fast to be resolved (c). (b) The polarization auto-correlation function (ACF) of (a) reveals a significant decay and oscillations with a 150 ms periodicity. The two horizontal dashed lines indicate the confidence interval (1σ). (d) The ACF of (c) also reveals a significant decay and oscillations. Inset: ACFs of 3 individual molecules (—) and an example without Na^+ (---) showing no correlation.[76]

The polarization response is equal regardless of the direction of rotation.

So far, any attempt to specifically inhibit the rotation of single F_0F_1-ATPases by dicyclohexylcarbodiimide (DCCD) failed.[72] It has been argued that this failure is due to the presence of detergent, in which F_0F_1 loses its structural integrity.[73] Here, with F_0F_1 being incorporated in liposomes, this problem has been overcome without the need for detergent, and rotation is clearly blocked after addition of 20 μM DCCD (Fig. 48(c)).

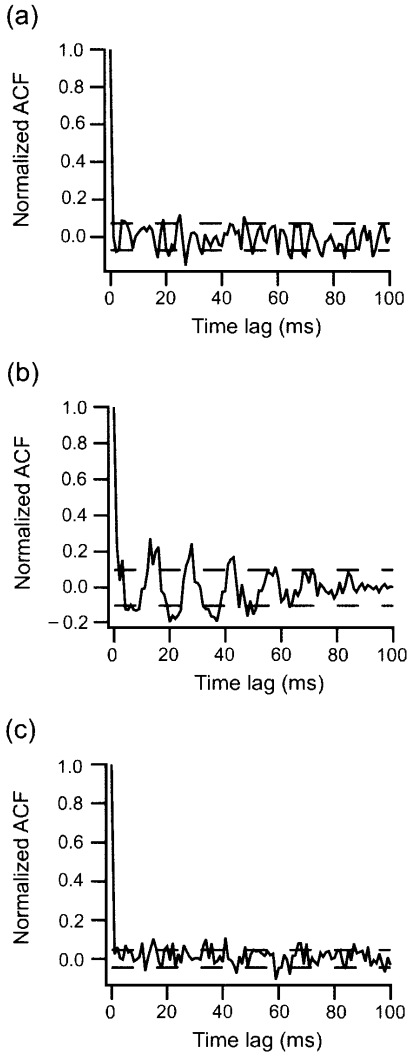

Fig. 48. Observation of rotation of F_0F_1 during ATP synthesis. F_0F_1 is incorporated in liposomes and bound to the glass surface. In the presence of a chemical Na^+ gradient alone, no rotation can be observed (a). After the membrane is charged, rotation of the F_0 is observed (b), and can be specifically blocked by adding 20 μM DCCD (c).[76]

According to the results of this study, without an applied membrane potential, no rotation is observed and thus no ATP synthesis takes place, again underpinning previous ensemble experiments.[65] After addition of valinomycin, which generates a membrane potential of about 95 mV (positive inside), 75% of the analyzed molecules rotate. Addition of 20 μM DCCD inhibits the rotation in over 90% of all cases analyzed.

In summary, the results obtained in this single-fluorophore polarization study are: (i) The step-wise rotation of the *c*-subunit in a functionally coupled F_0F_1 holoenzyme has been shown. The presence of sodium is proven to be an obligatory precondition for both rotation and ATP hydrolysis. (ii) For the first time, rotation during ATP synthesis could be observed in single F_0F_1 molecules. Enzymes incorporated in liposomes showed no rotation in the presence of an Na^+ concentration gradient alone. However, after applying a K^+/valinomycin diffusion potential, F_0F_1 rotated producing three ATP molecules per turn. Furthermore, it was possible to inhibit the rotation by the addition of DCCD, giving additional evidence that the enzyme used in this study was structurally and functionally the same as *in vivo* assembled F_0F_1 complexes.

Received January 3, 2003.

REFERENCES

1. Plakhotnik, T.; Donley, E.; Wild, U. Single-molecule Spectroscopy. *Annu. Rev. Phys. Chem*. **1997**, *48*, 181-212.
2. Rebane, K. K. *Impurity Spectra of Solids*; Plenum Press: New York, 1970.
3. *Persistent Spectral Hole-burning: Science and Applications*; Moerner, W. E. Ed.; Springer-Verlag: Berlin, 1988.
4. Nonn, T.; Plakhotnik, T. Fluorescence Excitation Spectroscopy of Vibronic Transitions in Single Molecules. *Chem. Phys. Lett*. **2001**, *336*, 97-104.
5. Donley, E. A.; Bonsma, S.; Palm, V.; Wild, V. B. U. P.; Plakhotnik, T. Zerophonon Lines of Single Molecules in Polyethylene Down to Millikelvin Temperatures. *J. Lumin*. **2000**, *87-89*, 109-114.
6. Nonn, T. Ph.D. thesis, ETH Zurich Diss. No. 14168, 2001.
7. de Vries, H.; Wiersma, D. A. Photophysical and Photochemical Molecular Hole Burning Theory. *J. Chem. Phys*. **1980**, *72*, 1851-1863.
8. Loudon, R. *The Quantum Theory of Light*; Oxford Science Publications, 1983.
9. Croci, M. Ph.D. thesis, ETH Zürich Diss. No. 12186, 1997.
10. Heitler, W. *The Quantum Theory of Radiation*; Dover Publ.:

1954, pp 181-189.
11. Rebane, K. K.; Rebane, I. Peak Value of the Cross-section of Zero-phonon Line's Absorption. *J. Luminescence* **1993**, *56*, 39-45.
12. Donley, E.; Plakhotnik, T. Spectral Diffusion in Polyethylene: Single-molecule Spectroscopy Studies Performed between 30 mK and 1.8 K. *J .Phys. Chem*. (In preparation) (2000), for a review on spectral diffusion see *Tunneling systems in amorphous and crystalline solids*; Esquinazi, P. Ed., Springer-Verlag: Berlin, 1999.
13. Pirotta, M.; Renn, A.; Werts, M. H. V.; Wild, U. P. Single Molecule Spectroscopy Perylene in the Shpol'skii Matrix *n*-nonane. *Chem. Phys. Lett*. **1994**, *250*, 576-582.
14. Pirotta, M. Ph.D. thesis, ETH Zürich Diss. No. 11887, 1998.
15. Thomas, I. Ph.D. thesis, ETH Zürich Diss. No. 12305, 1997.
16. Bach, H. Ph.D. thesis, ETH Zürich Diss. No. 12934, 1998.
17. Donley, E. A. Ph.D. thesis, ETH Zürich Diss. No. 13729, 2000.
18. Latychevskaia, T. Y. Ph.D. thesis, ETH Zürich Diss. No. 14425, 2002.
19. Plakhotnik, T. Single Molecule Spectroscopy: Maximum Emission Rate and Saturation Intensity. *Opt. Comm*. **1995**, *114*, 83-88.
20. Tamarat, P.; Maali, A.; Lounis, B.; Orrit, M. Ten Years of Single-molecule Spectroscopy. *J. Phys. Chem. A* **2000**, *104*, 1-16.
21. Güttler, F. Ph.D. thesis, ETH Zürich Diss. No. 10707, 1994.
22. Moerner, W. E.; Kador, L. Optical Detection and Spectroscopy of Single Molecules in a Solid. *Phys. Rev. Lett*. **1989**, *62*, 2535-2538.
23. Kador, L.; Horne, D. E.; Moerner, W. E. Optical Detection and Probing of Single Dopant Molecules of Pentacene in a *p*-terphenyl Host by Means of Absorption Spectroscopy. *J. Phys. Chem*. **1990**, *94*, 1237-1248.
24. Orrit, M.; Bernard, J. Single Pentacene Molecules Detected by Fluorescence Excitation in a *p*-Terphenyl Crystal. *Phys. Rev. Lett*. **1990**, *65*, 2716-2719.
25. Tchénio, P.; Myers, A. B.; Moerner, W. Dispersed Fluorescence Spectra of Single Molecules of Pentacene in *p*-Terphenyl. *J. Phys. Chem*. **1993**, *11*, 2491-2493.
26. Tchénio, P.; Myers, A. B.; Moerner, W. Vibrational Analysis of the Dispersed Fluorescence from Single Molecules of Terrylene in Polyethylene. *Chem. Phys. Lett*. **1993**, *213*, 325-332.
27. Myers, A. B.; Tchenio, P.; Moerner, W. E. Vibronic Spectroscopy of Single Molecules in Solids. *Abstract of Papers of the American Chemical Society* **1994**, 2, 208-233.
28. Fleury, L.; Tamarat, P.; Lounis, B.; Bernard, J.; Orrit, M. Fluorescence Spectra of Single Pentacene Molecules in *p*-Terphenyl at 1.7 K. *Chem. Phys. Lett*. **1995**, *236*, 87-95.
29. Kummer, S.; Kulzer, F.; Kettner, R.; Basché, T.; Tietz, C.; Glowatz, C.; Kryschi, C. Absorption, Excitation, and Emission Spectroscopy of Terrylene in *p*-Terphenyl: Balk Measurements and Single Molecule Studies. *J. Chem. Phys*. **1997**, *107*, 7673-7684.
30. Lu, H. P.; Xie, X. S. Single-molecule Spectral Fluctuations at Room Temperature. *Nature* **1997**, *385*, 143-146.
31. Bjorklund, G. C. Frequency-modulation Spectroscopy - New Method for Measuring Weak Absorptions and Dispersions. *Opt. Lett*. **1980**, *5*, 15-17.
32. Whittaker, M. G. E. A.; Bjorklund, G. C. Quantum-limited Laser Frequecy-modulation Spectroscopy. *J. Opt. Soc. Am. B* **1985**, *9*, 1510-1526.
33. Kador, L.; Latychevskaia, T.; Renn, A.; Wild, U. P. Absorption Spectroscopy on Single Molecules in Solids. *J. Chem. Phys*. **1999**, *111*, 8755-8758.
34. Moerner, W. E.; Huston, A. L. Phase Sensitive Detection of Persistent Holes Using Synchronous Ultrasonic Modulation. *Appl. Phys. Lett*. **1986**, *48*, 1181.
35. Schweiger, A.; Jeschke, G. *Principles of Pulse Electron Paramagnetic Resonance*; Oxford University Press: Oxford, 2001.
36. Sepiol, J.; Starukhin, A.; Kolos, R.; Latychevskaia, T.; Jasny, J.; Renn, A.; Wild, U. P. Detection and Spectroscopy of Single Molecules in Rare Gas Matrices: Dibenzanthanthrene in Krypton and Xenon. *Chem. Phys. Lett*. **1999**, *311*, 29-35.
37. Sepiol, J.; Starukhin, A.; Latychevskaia, T.; Jasny, J.; Renn, A.; Wild, U. P. Imaging and Spectroscopy of Terrylene Molecules Isolated in Vapor-deposited *n*-Alkane Matrices. *Chem. Phys*. **1999**, 247, 35-40.
38. Jasny, J.; Sepiol, J.; Irngartinger, T.; Traber, M.; Renn, A.; Wild, U. P. Fluorescence Microscopy in Superfluid Helium: Single Molecule Imaging. *Rev. Sci. Instrum*. **1996**, *67*, 1425-1430.
39. Islampour, R.; Hayashi, M. Analysis of Molecular Optical Spectra of Photosynthetic Raction Centers: Molecular Absorption, Hole Burning and Resonance Raman Spectra. *Advances in Multi-Photon Processes and Spectraoscopy* **1996**, *10*, 335-466.
40. Ambrose, W. P.; Basché, T.; Moerner, W. E. Detection and Spectroscopy of Single Pentacene Molecules in a *p*-Terphenyl Crystal by Means of Fluorescence Excitation. *J. Chem. Phys*. **1991**, *95*, 7150-7163.
41. Wild, U. P.; Croci, M.; Güttler, F.; Pirotta, M.; Renn, A. Single Molecule Spectroscopy: Stark Effect of Pentacene in *p*-Terphenyl. *Chem. Phys. Lett*. **1992**, *193*, 451-455.
42. Orrit, M.; Bernard, J.; Zumbusch, A.; Personov, R. Stark Effect of Single Molecules in a Polymer Matrix. *Chem. Phys. Lett*. **1992**, *196*, 595-600.
43. Brunel, C.; Tamarat, P.; Loiunis, B.; Woehl, J. C.; Orrit, M. Stark Effect on Single Molecules of Dibenzanthanthrene in a Naphthalene Crystal and in a *n*-Hexadecane Shpol'skii Matrix. *J. Phys. Chem. A* **1999**, *103*, 2429-2434.
44. Latychevskaia, T. Y.; Renn, A.; Wild, U. P. Higher-order Stark Effect on Single Molecules. *Chem. Phys*. **2002**, *282*, 109-119.
45. Hayashi, M. et al. Theory of the Stark Effect on Single Molecule Spectroscopy. *J. Chin. Chem. Soc*. **2002**, *49*, 797-804.

46. Anderson, P. W.; Halperin, B. I.; Varma, C. M. Anomalous Low-temperature Thermal Properties of Glasses and Spin Glasses. *Phil. Mag*. **1972**, *25*, 1-9.
47. Phillips, W. Thnneling States in Amorphous Solids. *J. Low. Temp. Phys*. **1972**, *7*, 351.
48. Reilly, P. D.; Skinner, J. L. Spectral Diffusion of Single-molecule Fluorescence – A Probe of Low Frequency Localized Excitations in Disordered Crystals. *Phys. Rev. Lett*. **1993**, *71*, 4257-2460.
49. Saven, J. G.; Skinner, J. L. A Molecular Theory of the Line-shape - Inhomogeneous and Homogeneous Electronic Spectra of Dilute Chromophores in Nonpolar Fluids. *J. Chem. Phys*. **1993**, *99*, 4391-4402.
50. Reilly, P. D.; Skinner, J. L. Spectroscopy of a Chromophore Coupled to a Lattice of Dynamic 2-Level System. 1. Absorption Line-shape. *J. Chem. Phys*. **1994**, *101*, 959-964.
51. Reilly, P. D.; Skinner, J. L. Spectroscopy of a Chromophore Coupled to a Lattice of Dynamic 2-Level System. 1. Spectral Diffusion Kernel. *J. Chem. Phys*. **1994**, *101*, 965-973.
52. Reilly, P. D.; Skinner, J. L. Spectral Diffusion of Individual Pentacene Molecules in *p*-Terphenyl Crystal: Stochastic Theoretical Model and Analysis of Experimental Data. *J. Chem. Phys*. **1995**, *102*, 1540-1552.
53. Villaeys, A. A.; Lin, S. H. Theory of Single Molecule Fluorescence in Large Molecular Systems. *J. Lum*. **2002**, *98*, 97-105.
54. Bardeen, J. Thnneling from a Many-particle Point of View. *Phys. Rev. Lett*. **1961**, *6*, 57.
55. Roy, D. K. *Quantum Mechanics Tunneling and Its Application*; World Scientific, 1986.
56. Eyring, H.; Lin, S. H.; Lin, S. M. *Basic Chemical Kinetics*; Wiley-International, 1980.
57. Lin, S. H. *J. Chem. Phys*. **1966**, *44*, 3756.
58. Huebner, C. G.; Renn, A.; Renge, I.; Wild, U. P. Direct Observation of the Triplet Lifetime Quenching of Single Dye Molecules by Molecular Oxygen. *J .Chem. Phys*. **2001***, 115*, 9619-9622.
59. Wilkens, S.; Capaldi, R. A. ATP Synthase's Second Stalk Comes into Focus. *Nature* **1998**, *393*, 29-32.
60. Stock, D.; Leslie, A. G.; Walker, J. E. Molecular Architecture of the Rotary Motor in ATP Synthase. *Science* **1999**, *286*, 1700-1705.
61. Abrahams, J. P.; Leslie, A. G.; Lutter, R.; Walker, J. E. Structure at 2.8 Å Resolution of f_1-atpase from Bovine Heart Mitochodria. *Nature* **1994**, *370*, 621-628.
62. Boyer, P. D. The ATP Synthase a Splendid Molecular Machine. *Annu. Rev. Biochem*. **1997**, *66*, 717-749.
63. Dimroth, P.; Wang, H.; Grabe, M.; Oster, G. Energy Transduction in the Sodium f-Atpase of Propionigenium Modestium. *Proc. Natl. Acad. Sci. USA* **1999**, *96*, 4924-4929.
64. Wang, H.; Oster, G. Energy Ttransduction in the f_1 Motor of ATP Synthase. *Nature* **1998**, *396*, 279-282.
65. Kaim, G.; Dimroth, P. ATP Synthesis by F-type ATP Synthase is Obligatorily Dependent on the Transmembrane Voltage. *EMBO J.* **1999**, *15*, 4118-4127.
66. Noji, H.; Yasuda, R.; Yoshida, M.; Kinosita, J. Direct Observation of the Rotation of F-1-ATPase. *Nature* **1997**, *386*, 299-302.
67. Hasler, K.; Engelbrecht, S.; Junge, W. Three-stepped Rotation of Subunits Gamma and Epsilon in Single Molecules of F-ATPase as Revealed by Polarized, Confocal Fluorometry. *FEBS Lett*. **1998**, *426*, 301-304.
68. Yasuda, R.; Noji, H.; Yoshida, M.; Kinosita, J.; Itoh, H. Resolution of Distinct Rotational Substeps by Submillisecond Kinetic Analysis of f_1-atapse. *Nature* **2001**, *410*, 898-904.
69. Adachi, K.; Yasuda, R.; Noji, H.; Itoh, H.; Harada, Y.; Yoshida, M.; Kinosita, J. Stepping Rotation of F-1-ATPase Visualized through Angle-resolved Single-fluorophore Imaging. *Proc. Natl. Acad. Sci. USA* **2000**, *97*, 7243-7247.
70 Yasuda, R.; Noji, H.; Kinosita, J.; Yoshida, M. F-1-ATPase is a Highly Efficient Molecular Motor That Rotates with Discrete 120 Degrees Steps. *Cell* **1998**, *7*, 1117-1124.
71. Kinosita, J.; Yasuda, R.; Noji, H.; Adachi, K. A Rotary Molecular Motor That Can Work at Near 100. **2000**, *355*, 473-489.
72. Sambongi, Y.; Iko, Y.; Tanabe, M.; Omote, H.; Iwamoto-Kihara, A.; Ueda, I.; Yanagida, T.; Futai, M. Mechanical Rotation of the c Subunit Oligomer in ATP Synthase (FOF1): Direct Observation. *Science* **1993**, *286*, 1722-1724.
73. Tsunoda, S. P.; Aggeler, R.; Noji, H.; Kinosita, J.; Yoshida, M.; Capaldi, R. A. Observations of Rotation within the FOFI-ATP Synthase: Deciding between Rotation of the F(O)c Subunit Ring and Artifact. *FEBS Lett*. **2000**, *470*, 244-248.
74. Schulenberg, B.; Capaldi, R. A. The Epsilon Subunit of the F1F0 Complex of Escherichia coli - Cross-Linking Studies Show the Same Structure in Situ as When Isolated. *J. Biol. Chem*. **1999**, *40*, 28351-28355.
75. Panke, O.; Gumbiowski, K.; Junge, W.; Engelbrecht, S. F-ATPase: Specific Observation of the Rotating c Subunit Oligomer of EFoEF1. *FEBS Lett*. **2000**, *1*, 34-38.
76. Prummer, M. Ph.D. thesis, ETH Zürich Diss. No. 144444, 2002.
77. Kaim, G.; Prummer, M.; Sick, B.; Zumofen, G.; Renn, A.; Wild, U. P.; Dimroth, P. Coupled Rotation within Single F0F1 Enzyme Complexes during ATP Synthesis or Hydrolysis. *FEBS Lett*. **2002**, *1-3*, 156-163.
78. Prummer, M.; Hecht, B.; Wild, U. P. Observing Single F0F1 ATP Synthases at Work. *Biophys. J.* **2002**, 82, 0.
79. Chipot, C.; Angyan, J. G.; Ferenczy, G.; Scheraga, H. A. *Stochastics Problems in Physics and Astronomy*; Review of Modern Physics, 1943, pp 1-89.
80. Reif, F. *Fundamentals of Statistical and Thermal Physics*; McGraw-Hill, 1985.
81. Wild, U. P. From Single Molecule Spectroscopy to the Molecular Computer. Proc. Symp. on Photo-Reactive Materials for Future Ind., Tokio, 1993, pp 483-494.